Department of Materials Science and Engineering

Role of twin boundary mobility in performance of the Ni-Mn-Ga single crystals

Ilkka Aaltio

Aalto University

DOCTORAL DISSERTATIONS

Aalto University publication series
DOCTORAL DISSERTATIONS 109/2011

Role of twin boundary mobility in performance of the Ni-Mn-Ga single crystals

Ilkka Aaltio

Doctoral dissertation for the degree of Doctor of Science in Technology to be presented with due permission of the School of Chemical Technology for public examination and debate in Auditorium V1 at the Aalto University School of Chemical Technology (Espoo, Finland) on the 11th of November 2011 at 12 o'clock noon.

Aalto University
School of Chemical Technology
Department of Materials Science and Engineering
Research Group for Advanced and Functional Materials

Supervisor
Prof. Simo-Pekka Hannula

Instructor
Prof. Simo-Pekka Hannula

Preliminary examiners
Prof. Eduard Cesari
Universitat de les Illes Balears, Palma de Mallorca, Spain

Associate Prof. Liu Yong
Nanyang Technological University, Singapore

Opponents
Prof. Manuel Barandiarán
Universidad del Pais Vasco (UPV-EHU), Bilbao, Spain

Aalto University publication series
DOCTORAL DISSERTATIONS 109/2011

ISBN 978-952-60-4343-2 (pdf)
ISBN 978-952-60-4342-5 (printed)
ISSN-L 1799-4934
ISSN 1799-4942 (pdf)
ISSN 1799-4934 (printed)

Unigrafia Oy
Helsinki 2011

Finland

The dissertation can be read at http://lib.tkk.fi/Diss/

Aalto University

Abstract

Aalto University, P.O. Box 11000, FI-00076 Aalto www.aalto.fi

Author
Ilkka Aaltio

Name of the doctoral dissertation
Role of twin boundary mobility in performance of the Ni-Mn-Ga single crystals

Publisher School of Chemical Technology

Unit Department of Materials Science and Engineering

Series Aalto University publication series DOCTORAL DISSERTATIONS 109/2011

Field of research Materials Science

Manuscript submitted 24 May 2011 **Manuscript revised** 13 October 2011

Date of the defence 11 November 2011 **Language** English

☐ **Monograph** ☒ **Article dissertation (summary + original articles)**

Abstract

Ni-Mn-Ga alloys have attracted great interest for more than ten years from the scientific community because of the exceptional properties of their twinned martensitic microstructure, combined with their magnetic properties such as high anisotropy. The high mobility of their martensitic twin variant boundaries enables the magnetic shape memory actuation and the high mechanical vibration damping capacity, to name just a few applications. Their material properties are in several ways unique, such as the large magnetic-field-induced strain of several per cent operating at frequencies of several hundred Hz. The most mobile twin boundaries have been found in high-quality single crystals. However, the twin boundary mobility of different crystals often varies significantly. It may even vary in the same crystal, which is not favorable for their practical use. In this work, twin mobility of several types of Ni-Mn-Ga single crystals is studied under monotonic uniaxial and shear loading as well as in dynamic loading at different temperatures. Furthermore, the performance of the material is studied by mechanical and magneto-mechanical cycling of the twin boundaries to reveal changes in the material properties. The results show that the stress needed for the twin mobility in both uniaxial and shear mode can be very low. In the shear mode the twin boundary motion can start even at 0.07 to 0.23 MPa stress. However, the stress onset for the twin boundary motion in the single variant state can be more than a decade higher than in the state with existing twin boundaries. As demonstrated in this Thesis by 2 x 10^9 cycles at 2 % strain peak-to-peak, 10M Ni-Mn-Ga has potentially a long fatigue life, however several reasons which may reduce their long-term performance are confirmed or proposed.

Keywords Ni-Mn-Ga, martensite, twinning, fatigue, ferromagnetic shape memory, damping

ISBN (printed) 978-952-60-4342-5 **ISBN (pdf)** 978-952-60-4343-2

ISSN-L 1799-4934 **ISSN (printed)** 1799-4934 **ISSN (pdf)** 1799-4942

Location of publisher Espoo **Location of printing** Helsinki **Year** 2011

Pages 152 **The dissertation can be read at** http://lib.tkk.fi/Diss/

Tekijä
Ilkka Aaltio

Väitöskirjan nimi
Kaksosrajojen liikeherkkyyden vaikutus Ni-Mn-Ga-yksikiteiden käyttöominaisuuksiin

Julkaisija Kemian tekniikan korkeakoulu

Yksikkö Materiaalitekniikan laitos

Sarja Aalto University publication series DOCTORAL DISSERTATIONS 109/2011

Tutkimusala Materiaalitiede

Käsikirjoituksen pvm 24.05.2011 **Korjatun käsikirjoituksen pvm** 13.10.2011

Väitöspäivä 11.11.2011 **Kieli** Englanti

☐ **Monografia** ☒ **Yhdistelmäväitöskirja (yhteenveto-osa + erillisartikkelit)**

Tiivistelmä

Ni-Mn-Ga-seokset ovat kiinnostaneet tutkijoita jo yli kymmenen vuoden ajan, sillä niissä martensiittinen kaksostunut mikrorakenne on yhdistynyt tiettyihin magneettisiin ominaisuuksiin, kuten suureen anisotropiaenergiaan. Martensiitin helposti liikkuvien kaksosrajojen ansiosta näitä seoksia voidaan käyttää esimerkiksi magneettisesti ohjattavina aktuaattorimateriaaleina sekä mekaanisen värähtelyn vaimennukseen. Yksikiteisessä Ni-Mn-Ga:ssa kaksorajojen liikkuvuus voi vaihdella eri kiteiden välillä ja jopa samassa kiteessä. Tässä työssä tutkitaan eri tyyppisiä Ni-Mn-Ga yksikiteitä sekä monotonisessa kuormituksessa (aksiaali- ja leikkausmuodonmuutostilassa) että dynaamisessa kuormituksessa värähtelynvaimennusmittausten ja väsymiskokeiden avulla. Tulokset osoittavat, että kaksosrajojen liike voi alkaa hyvin pienellä, jopa 0.07-0.23 MPa jännityksellä. 10M martensiittityypin Ni-Mn-Ga kide kesti parhaimmillaan väsymiskuormituksessa 2 x 10^9 sykliä 2 % (p-p) venymällä. Väsymiskestävyys vaihtelee eri kiteiden välillä ja työssä esitetään useita syitä tälle vaihtelulle.

Avainsanat Ni-Mn-Ga, martensiitti, kaksostuminen, väsyminen, muistimetalli, sisäinen kitka

ISBN (painettu) 978-952-60-4342-5 **ISBN (pdf)** 978-952-60-4343-2

ISSN-L 1799-4934 **ISSN (painettu)** 1799-4934 **ISSN (pdf)** 1799-4942

Julkaisupaikka Espoo **Painopaikka** Helsinki **Vuosi** 2011

Sivumäärä 152 **Luettavissa verkossa osoitteessa** http://lib.tkk.fi/Diss/

Preface

The present work was conducted at Aalto University (previously Helsinki University of Technology), Department of Materials Science and Engineering. I wish to express my deepest gratitude to my supervisor Prof. Simo-Pekka Hannula for his encouraging attitude to my work, our fruitful discussions, and for providing me with suitable working conditions. I wish to sincerely thank my colleague Dr. Outi Söderberg for her valuable advice with regard to the scientific work and the realization of this Thesis. In addition, I wish to thank my colleagues Dr. Yanling Ge and Dr. Alexei Sozinov for their valuable advice and assistance with the research work. The co-authors of the Publications are gratefully acknowledged for their contributions. Several other persons have provided me with valuable help in performing this work: Dr. Juhani Tellinen, Olli Mattila, Natalya Lanska, Prof. Ari Lehto, Prof. Toivo Katila, Prof. Veikko Lindroos, Prof. Hannu Hänninen and the late Prof. Juha Pietikäinen. Furthermore, I wish to thank the staff of the Department of Materials Science and Engineering for their positive attitude and assistance. In particular I wish to thank Pirjo Korpiala for her practical help in the laboratory. For the part of the work which was conducted on my visit to UCLA I wish to acknowledge Prof. Greg P. Carman.

I wish to thank my colleague and friend Dr. Kari Ullakko for introducing me to the MSM topic back in 1995, and for our inspiring research collaboration thereafter, which eventually attracted me to work for many years in the company Adaptamat that we established together.

For the valuable financial support I wish to acknowledge Tekes (the Finnish Funding Agency of Technology and Innovation), the Academy of Finland, Jenni and Antti Wihuri Foundation and the Finnish companies Metso Paper, Adaptamat, Teknikum and Outotec.

I wish to gratefully thank my dear wife Christina for her love and incredible support with my work, as well as my children Sara, Juhana and Markus for their kind understanding. Finally, I wish to thank my par-

ents Juhani and Sirkka for their invaluable encouragement and support. Without you this work would never have been realized.

Helsinki, October 20, 2011,

Ilkka Ilari Aaltio

List of Publications

This Thesis consists of an overview and of the following publications which are referred to in the text by their Roman numerals.

I I. Aaltio, O. Heczko, O. Söderberg and S-P. Hannula. Magnetically Controlled Shape Memory Alloys. In *CRC Handbook "'Smart Materials"'*, M. Schwartz (Editor), pp. 20-1–20.8, 2009.

II I. Aaltio, O. Söderberg, Y. Ge, S-P. Hannula. Twin boundary nucleation and motion in Ni-Mn-Ga magnetic shape memory material with a low twinning stress. *Scripta Materialia*, 62, pp. 9-12, Doi:10.1016/j.scriptamat.2009.09.012, September 2010.

III I. Aaltio, M. Lahelin, O. Söderberg, O. Heczko, B. Löfgren, Y. Ge, J. Seppälä and S-P. Hannula. Temperature dependence of the damping properties of Ni-Mn-Ga alloys. *Materials Science and Engineering: A*, 481-482, pp. 314-317, Doi: 10.1016/j.msea.2006.12.229, December 2008.

IV I. Aaltio, K. P. Mohanchandra, O. Heczko, M. Lahelin, Y. Ge, G. P. Carman, O. Söderberg, B. Löfgren, J. Seppälä, S-P. Hannula. Temperature dependence of mechanical damping in Ni-Mn-Ga austenite and non-modulated martensite. *Scripta Materialia*, 59, pp. 550-553, Doi: 10.1016/j.scriptamat.2008.05.005, May 2008.

V I. Aaltio, Y. Ge, X. W. Liu, O. Söderberg and S-P. Hannula. Effect of magnetomechanical cycling on 10M Ni-Mn-Ga magnetic shape memory material. In *G. B. Olson, D. S. Liebermann, A. Saxena (Editors), Proceedings of the International Conference on Martensitic Tranformations ICOMAT 2008*, pp. 487-491, ISBN 978-0-87339-745-2, 2009.

VI I. Aaltio, A. Soroka, Y. Ge, O. Söderberg and S-P. Hannula. High-cycle fatigue of 10M Ni-Mn-Ga magnetic shape memory alloy in reversed mechanical loading. *Smart Materials and Structures*, 19, 075014, 10 pp,
Doi:10.1088/0964-1726/19/7/075014, June 2010.

Brief Description of the Publications

Publication I: "Magnetically Controlled Shape Memory Alloys"

In this Publication a critical review of magnetically controlled shape memory alloys is presented. Ni-Mn-Ga magnetic shape memory alloys are used as the example material for describing the operating principle of magnetic shape memory actuators and the magneto-mechanical behavior of these materials. The importance of the twin boundary mobility and its utilization for several purposes, e.g. actuation, sensing, power generation and vibration damping is pointed out.

Publication II: "Twin boundary nucleation and motion in Ni-Mn-Ga magnetic shape memory material with a low twinning stress"

Twin boundary mobility of 10M $Ni_{50.1}Mn_{27.7}Ga_{22.2}$ single crystal stick was studied by mechanical compression and magnetic measurements. The different variant states were created by applying a magnetic field.

The results of the Publication reveal the influence of the pre-existing twin variant structure to twin boundary motion. It was shown that in a low twinning stress 10M Ni-Mn-Ga, the stress onset needed for the motion of the twin boundary in the (essentially) single variant state is remarkably higher than that in the two variant state with existing twin boundaries. This was confirmed by the magnetic switching field measurements. It is proposed that the stress onset is caused by the nucleation of a second variant and the formation of the related twin boundary. Furthermore, the results suggest that the mechanism for a shape change of the MSM material may be different in different variant states.

Publication III: "Temperature dependence of the damping properties of Ni-Mn-Ga alloys"

Temperature dependency of the damping capability of mechanical vibration was studied of 10M, NM and mixed martensites by the dynamical mechanical analysis (DMA) and the temperature dependency of twinning stress and strain was determined. In the martensite state damping (i.e., loss tangent $\tan\delta$) of all the Ni-Mn-Ga alloys tested was found to increase with increasing temperature up to the parent phase region, where the $\tan\delta$ dropped drastically. It is notable that the twinning stress and the maximum twinning strain of martensite decreases with decrease of the storage modulus. Because of the lower phase transformation temperature the drop in the damping in the 10M alloy takes place at a lower temperature than in the NM alloy.

The results of this Publication show the temperature dependency of twin boundary motion and damping in the Ni-Mn-Ga martensites. Based on the results, it is suggested that the high damping of Ni-Mn-Ga single crystals is related to the motion of twin or phase boundaries.

Publication IV: "Temperature dependence of mechanical damping in Ni-Mn-Ga austenite and non-modulated martensite"

In order to confirm the role of twin boundary movement in damping, the stress amplitude dependency of the loss tangent and the dynamic modulus of NM $Ni_{52.3}Mn_{27.4}Ga_{20.3}$ was studied at various temperatures by the DMA method.

In the martensite phase, $\tan\delta$ increases with stress amplitude, and thus with strain amplitude as it is experimentally confirmed elsewhere in this Thesis, whereas in the parent phase $\tan\delta$ remains at a low level. The damping in NM Ni-Mn-Ga martensite only increases above a threshold stress level, namely the twinning stress of the material. The results of this Publication confirm that in the martensite phase the high damping is mainly due to the hysteretic motion of twin boundaries.

Publication V: "Effect of magnetomechanical cycling on 10M Ni-Mn-Ga magnetic shape memory material"

Response of the 10M material to magneto-mechanical uniaxial cycling was studied in order to understand the influence of long term cycling on the twin boundary mobility.

When the twin boundaries are driven back and forth, the material withstands a large number of cycles without failure, but at the same time some microcracks developed on the specimen surface. The twinning stress increased by about 10 % during cycling of over 200 $\cdot 10^6$ cycles when calculated by the displacement-current cycle of the actuator. It was discovered that despite the large scatter of the results, the magnetic field induced strain is decreased because of reduction of twin boundary mobility associated to surface deformation induced by wear.

Publication VI: "High-cycle fatigue of 10M Ni-Mn-Ga magnetic shape memory alloy in reversed mechanical loading"

The Publication focuses on the response of the 10M materials to long-term mechanical cycling. Tests were conducted with ten 10M samples using a specifically made cycling test apparatus. The major changes of the material properties, as well as microstructure and crack growth, are presented.

The mechanical cycling tests confirmed the nucleation and growth of the fatigue cracks, but demonstrated also a fatigue life up to $2 \cdot 10^9$ cycles without failure of the sample. The slope of the dynamic stress-strain loop was increasing with the number of cycles in the range beyond several tens of millions, which correlates with increased twin boundary density. The fatigue-induced cracks and fracture surfaces were studied. It is shown that the material withstands a large number of cycles without failure when the straining is realized by the cyclic twin boundary movement. The fatigue life of the material is reduced by growth of fatigue cracks and changes in the actively moving twin boundary area. Possible reasons for the evolution of cracks are proposed elsewhere in this Thesis.

Author's Contribution

The Author is the responsible author and has contributed the majority of the writing work of all Publications (I to VI) presented in this Thesis. Of the experimental work, he has been responsible for the mechanical twinning stress measurements, magnetic measurements, microstructural characterization, X-ray diffraction studies and part of the presented dynamical mechanical analysis (DMA). In addition, he has been responsible for conducting the shear tests and the magneto-mechanical fatigue tests and for the design and construction of the specific equipment for these purposes. The Author supervised the M. Sc. Thesis work concerning the mechanical cycling of 10M Ni-Mn-Ga, and contributed to the analysis of the fatigue results and the studies of the fatigue-induced microstructural changes of the material.

In addition to participating in the preparation of the manuscripts of the Publications, the co-authors have contributed the following parts:

- Prof. S-P. Hannula provided important scientific guidance for the research work and contributed to the analysis of the fatigue-induced cracks and to the studies of twin boundary mobility.

- Prof. J. Seppälä and Dr. B. Löfgren participated in the planning of the experiments and preparation of the manuscript of Publication III.

- Prof. G. P. Carman and Dr. K. P. Mohanchandra provided important assistance to the Author in conducting the DMA and DSC studies at the University of California Los Angeles (UCLA).

- Dr. O. Söderberg provided important scientific guidance for the work and conducted a part of the Ni-Mn-Ga characterization. She offered an important author contribution to the review article (Publication I).

- Dr. Y. Ge contributed to the X-ray diffraction and scanning electron microscope studies, as well as the analysis of the fatigue cracks.
- Dr. X. W. Liu conducted the SEM studies of Publication V together with the Author.
- Dr. J. Tellinen conducted part of the magneto-mechanical cycling tests of Publication V and contributed to the design of the magneto-mechanical cycling system.
- Dr. O. Heczko provided expertise to the Author with the analysis of the magnetic measurement results.
- M. Sc. M. Lahelin conducted the DMA measurements in Publication III and participated in the DMA analysis.
- M. Sc. A. Soroka conducted the mechanical cycling experiments and part of the microstructural characterization of Publication VI. He designed the mechanical fatigue test apparatus as a part of his M. Sc. Thesis.

Professor Simo-Pekka Hannula

Espoo, May 23, 2011

Contents

List of symbols

a, b and c	lattice parameters
A_f	austenite finish temperature
A_s	austenite start temperature
d	diameter
η_1	twinning shear direction
η_2	conjugate twinning shear direction
(e/a)	electron to atom ratio
ϵ_0	(lattice dependent) maximum linear twinning strain
$\Delta\epsilon_a$	strain amplitude (peak-to-peak)
$\epsilon_{plateau}$	shear strain of the twinning plateau
E_0	barrier energy
E	modulus of elasticity
γ	shear strain
γ_0	(lattice dependent) maximum shear twinning strain
f_1 and f_2	relative volume fractions of twin variants
F	applied force
h	magnetic field energy or magnetic field intensity
H	habit plane
H_{appl}	applied magnetic field
H_{sw}	switching magnetic field
K_1	twin plane or magnetic anisotropy constant
K_2	conjugate twin plane
K_U	uniaxial magnetic anisotropy constant
l	length
M	magnetization
M_f	martensite finish temperature
M_s	martensite start temperature
M_S	saturation magnetization
P	displacement plane or plane of shear in twinning

σ_{ext}	external applied compressive stress
σ_{mag}	magnetic field induced stress
σ_{mech}	internal mechanical stress (at H_{appl}=0)
σ_{start}	uniaxial stress at the onset of twin boundary motion
σ_{finish}	uniaxial stress at the end of the twinning plateau
σ_{tw}	twinning stress
s	strain energy
T_C	the Curie temperature
τ_{start}	shear stress at the onset of twin boundary motion
τ_{finish}	shear stress at the end of the twinning plateau
τ_t	twinning shear stress
$\tan\delta$	loss tangent

List of abbreviations

$10M$	5-layered modulated martensite (in literature also referred to as $5M$)
$14M$	7-layered modulated martensite (also referred to as $7M$)
BCC	body centered cubic
DMA	dynamical mechanical analysis
EDS	electron dispersive x-ray microanalysis
FCC	face centered cubic
FCT	face centered tetragonal
$GPSF$	generalized planar stacking fault energy
HCP	hexagonal close packed
$MFIS$	magnetic field induced strain
MSM	magnetic shape memory (also referred to as $FSMA$)
MT	martensite transformation
NM	non-modulated martensite (also referred to as $2M$ or T martensite)
SEM	scanning electron microscope
SMA	shape memory alloy
VSM	vibrating sample magnetometer
XRD	X-ray diffraction
XRF	X-ray fluorescence

List of Figures

On front cover: A detail of a SEM image (SEI) of the fracture surface of a single crystal 10M $Ni_{50.0}Mn_{28.3}Ga_{21.7}$ fatigue specimen (Courtesy of Dr. Y. Ge, Aalto University, published with permission).

List of Tables

1 Introduction

1.1 Martensite phases and twinning in Ni-Mn-Ga alloys

1.1.1 Martensite in Ni-Mn-Ga alloys

Martensite phase transformation (MT) is a diffusionless solid state shear transformation, where the crystal lattice is dilatated from the parent phase (usually the symmetric face centered cubic (FCC) austenite structure) to a lower symmetry martensite structure during cooling or by external stress [1]. It occurs by a displacive shear-like mechanism involving a minor (less than the interatomic distance in the crystal) shift of atomic positions, driven by the lower level of free energy of martensite in comparison to that of the parent phase. The martensite transformation from the cubic parent phase may occur in different ways, which are defined by the transformation matrix, resulting in different martensite structures such as the monoclinic (found, e.g, in Ni-Ti), orthorhombic (e.g., Cu-Al-Ni), etc. [2]. Due to the asymmetrical crystal structure of martensite, several regions with different orientations in the martensite of the same crystallographic structure are usually formed in MT. These differently oriented regions are called martensite variants (i.e., martensite correspondence variants) [1, 3]. The adjacent variant regions are separated by a coherent variant boundary, which allows the crystal structure to continue unbrokenly from one variant to the neighboring variant. The possible number of differently oriented variants is limited by the crystal structure.

When the material is cooled over the phase transformation regime, a self-accommodated martensite variant structure is formed in such a way that the lattice dilatations of different variants inside the material tend to compensate for one another. If the martensite material is heated, it transforms back to the parent phase of the original orientation by reverse transformation. The martensite transformation starting temperature M_s and the finishing temperature M_f vary to a large extent from one alloy to

another, as well as the starting and completion temperatures for the reverse transformation (A_s, A_f). There is a hysteresis between the forward and the reverse transformations.

As discussed above, in addition to temperature, martensitic reaction may also be triggered by the external stress on the parent phase [4], or in the case of ferromagnetic martensite, by applied magnetic field H_{appl}. Transformation may also be induced by the combination of these parameters, i.e., temperature-stress [5], temperature-magnetic field [6], or magnetic field-stress [7]. Triggering by the applied magnetic field or by stress is possible only in a limited temperature window. For example, the magnetic field-induced reverse transformation in $Ni_{45.5}Co_5Mn_{37.6}In_{13.3}$ was demonstrated at 9 K below A_s, and the required field strength was rather high H_{appl} = 2388 $\frac{kA}{m}$ (approximately 3 T) [8]).

During cooling, before the start of martensite reaction, there may be a premartensitic transformation, as in Ni_2MnGa [9]. This has been explained by the phonon softening, which is expected to increase the amplitude of the lattice vibrations [10], promoting the vibration damping of the parent phase.

In 1903, at the same time when the German engineer Adolf Martens (1850-1914) worked with martensite, F. A. Heusler published results of a new kind of metal alloy Cu_2MnAl that after quenching and tempering in the ordered state exhibited ferromagnetism, despite it consisting of paramagnetic elements Cu, Mn and Al [11]. The alloy, which was named after Heusler, was to be used for the construction parts made by rolling. The crystal structure of the Heusler alloy Cu_2MnAl was determined as an ordered $L2_1$ according to the Structure Report notation [12]. It has in the ordered state a distinctive sublattice composition of four interpenetrating FCC-sublattices [13]. Later this kind of crystal structure has been found in several metal alloys (or intermetallic compounds) and with the composition of the type X_2YZ which is generally referred to as the Heusler structure.

At first, research of the Heusler alloys at first only concentrated on studying the interatomic distances on the ferromagnetic properties, and on determining the alloy valences from their magnetic properties. Ni_2MnGa was reported in 1960 by Hames as being at room temperature a ferromagnetic Heusler alloy [14] with strong ferromagnetic properties based on the Mn-Mn-atomic distance of a specific range. However, many details such as the contribution of Ni on the ferromagnetic properties of the alloy were

not entirely clear at that time. Lattice structure and magnetic properties were studied by Webster [15] and atomic ordering by Soltys [16]. The latter found that the Ga-atoms could be ordered with heat treatment near 1173 K for several tens of hours in a protective atmosphere followed by quenching. The highly ordered $L2_1$ Heusler crystal structure (austenite) was also described by Soltys. The Ga atoms are placed at all eight corners and at the six face centers of the cubic unit cell. The Mn atoms are placed in between the Ga atoms, i.e., one at the middle of each edge and one Mn at the center of the unit cell. The Ni atoms have positions in the $<\frac{1}{4}\frac{1}{4}\frac{1}{4}>$ sites, i.e., at the center of each eight cubic sub-unit of the unit cell. According to Webster *et al.* [13] the M_s temperature of stoichiometric Ni_2MnGa is 202 K and the Curie temperature (T_C) 376 K. Tetragonal martensite with a = 5.920 Å and c = 5.566 Å was found to appear in the MT.

In order to control the crystal structure of the alloy, the high temperature properties should be known. The melting temperature of the stoichiometric Ni_2MnGa is 1382 K, while those of the off-stoichiometric alloys vary typically from 1347 K of $Ni_{50}Mn_{35}Ga_{15}$ to 1396 K of $Ni_{50}Mn_{20}Ga_{30}$ [17]. The Ni_2MnGa alloy shows a disordered $B2'$ phase above 1071 K [13, 17]. In $B2'$, the Mn and Ga atoms have a random lattice site distribution, contrary to the ordered phase ($L2_1$) which was discussed before. For the non-stoichiometric Ni-Mn-Ga alloys, the $L2_1 - B2'$ transformation temperature depends on the chemical composition. It is in the range from 800 to 1000 K [17, 18] depending on the Ni/Mn ratio [19]. The ordering takes place by diffusion. Diffusivity of Ni and Mn is higher than that of Ga in the temperature range of 954 - 1191 K. Diffusion in the Ni-Mn-Ga alloys has been proposed to involve vacancies and to occur by a coupled mechanism [20]. Thus the above mentioned long ordering heat treatment is usually needed for obtaining a highly ordered structure.

As the densely packed Heusler $L2_1$ structure is commonly defined for the stoichiometric composition, in the off-stoichiometric Ni-Mn-Ga alloys an incompletely ordered structure is expected to appear at the $B2' - L2_1$ transformation, since the number of atoms does not equal the number of available Heusler lattice sites for these elements. Since the Ni-lattice remains intact in this transformation, in the case of Ni $\neq$ 50 at-% the resulting $L2_1$ structure may be assumed to contain a discontinuous Ni-sublattice, with an excess of Mn or Ga atoms or vacancies. The ordering of the $L2_1$ structure affects to a great extent the properties of the martensite, since the ordering of the parent phase is inherited in the MT. The

ordering of the off-stoichiometric alloys is today not entirely known in detail, but studies have been conducted of this topic [21, 22]. Atomistic simulation has shown that the Mn excess favors the antiferromagnetic alignment with respect to neighboring Mn atoms by $2.5\mu_B$ per each excess Mn atom [23]. It has been suggested that the excess Ni prefers to occupy the Mn sites, reducing the lattice distortion, by driving the displaced Mn to the Ga sites of the compound $Ni_9Mn_4Ga_3$ [22]. The most applicable multifunctional properties, e.g., a combination of ferromagnetic state, reasonably high A_s combined with the Curie temperature (T_C) around 373 K, and a fluent mobility of twins, have been found in the off-stoichiometric Ni-Mn-Ga alloys with excess Mn and deficient Ga, such as $Ni_{50}Mn_{28}Ga_{22}$. The martensite transformation temperature has been found to increase with the electron to atom ratio (e/a), whereas the Curie temperature is less sensitive to compositional changes, being usually in the range of 360 to $380K$ [24, 25]. T_C of Ni_2MnGa is also relatively insensitive to compressive stress, as it grows with stress only at a rate of $dT_C/d\sigma \approx 5$ K/GPa [26]. The degree of atomic ordering of the $L2_1$ phase has been shown to increase T_C in the alloy $Ni_{51.2}Mn_{31.1}Ga_{17.7}$ by ≈100 K, evolving in a parallel way with the observed intermartensitic transformation, whereas in $Ni_{53.1}Mn_{26.6}Ga_{20.3}$ the effect is less (≈10 K) [27].

Different martensite structures exist in the Ni-Mn-Ga alloys of different chemical compositions. A correlation has been found between the electron to atom ratio (e/a) of the alloy and its tetragonality and the martensite type [28]. Orthorhombic 7-layered (14M, also referred to as 7M) which exists in e.g. $Ni_{48.8}Mn_{29.7}Ga_{21.5}$ has the maximum strain ϵ_0 of 0.106, and tetragonal, non-layered, non-modulated (NM, also referred to as 2M, or T) martensite in e.g. $Ni_{52.1}Mn_{27.3}Ga_{20.6}$ has $\epsilon_0 \approx 0.2$ [29, 30]. Density functional calculations of Ni_2MnGa have shown that the energy of the modulated structure is higher than in the NM martensite [25]. Intermartensitic transformation may exist as well at certain compositions [31]. When cooled the $Ni_{50.5}Mn_{30.4}Ga_{19.1}$ alloy transforms in a solid state from the non-ordered one to cubic structures and then to different martensites in the following order: $B2' \rightarrow L2_1 \rightarrow 10M \rightarrow 14M \rightarrow NM$. The crystal structures of martensites have been studied in many publications, e.g., [32, 33, 34]. In the X-ray diffraction (XRD) study of constrained epitaxial Ni-Mn-Ga thin film grown on $MgO_{(100)}$ substrate [35] it was noted that the 14M martensite consists of nanotwinned layers of the 5-layered (10M) and the non-modulated (NM) martensites. This has been explained by the

adaptive martensite concept introduced by Khachaturyan *et al.* [36]. The macroscopic NM variants connect to the nanotwinned 10M and the NM martensites by a branching mechanism. The adaptive martensite concept may be applied to the well-known intermartensitic transformations. The adaptive 14M structure has been stated to be metastable [36] - in contrary to the stable 10M and NM martensite structures. In the case of thin film, the constraint caused by the substrate would have promoted the metastable 14M phase. However, since experimental studies of the bulks with the stable 14M phase have been presented in many publications, the reasons for its stability is not entirely clear. For example, it has been suggested that there would exist an energy barrier related to the repulsive forces between twin boundaries and the lattice defects [35].

The twin plane between the neighboring martensite variants in the 10M martensite is described using either the crystal space group $Fmmm$ (space group number 69) or alternatively $I4/mmm$ (space group number 139) [33]. The first way has been frequently used due to the adequate matching of the easy axis of magnetization with the [001] crystal direction [33], and it is used also in this Thesis. In the $Fmmm$ system, the twin plane is {101}, i.e., (101), $(10\bar{1})$, (011) or $(01\bar{1})$. Detailed neutron diffraction investigations have shown that the unit cell of the martensite may be only approximately described using the $Fmmm$ space group 69 unit cell and a monoclinic presentation is necessary when described accurately [28]. When the close to tetragonal [37, 34] martensite is transformed from the $Ni_2MnGa\ FCC$ parent phase $(L2_1)$, a five layered periodic superstructure is formed in the martensite by shuffling along the (110) plane in the $[1\bar{1}0]_m$ direction [38]. This 5-layered $(5M)$ modulated martensite is detectable from the four extra spots in the X-ray diffraction (XRD) pattern. This superstructure is repeated over 10 atomic planes along the (110) plane, which is why this same type of martensite is in many publications called 10M, where the letter M denotes a monoclinic crystal structure in Ramsdel notation. In a more detailed study, the shuffling has been concluded to be a sum of two different contributions: the wave-like modulation and additional not-wave-like tetrahedral distortions of Ga and Mn, including radial and angular parts [39]. However, the amplitudes of the tetrahedral distortions are only about 1% of the modulation amplitude. $10M$ martensite is found in the stoichiometric and off-stoichiometric alloys such as $Ni_{49.2}Mn_{29.6}Ga_{21.2}$, where $\epsilon_0 = (1 - (c/a))$ of 0.058.

1.1.2 Twinning mechanisms

Twins are classically defined as two adjacent crystals, with their lattices related either by a reflection in some plane or by a rotation of 180° around some axis. The planar interface between the adjacent twins is called the twin boundary. The main twinning mechanisms are mechanical and thermally induced twinning. Mechanical twinning occurs when atom movements in a crystal results in a new crystal of different orientation but identical structure. Together with slip it is the major deformation mode allowing a shape change under stress at temperatures below which individual atoms are mobile. Thermal twins are formed by the thermal stresses and they are basically mechanical in nature, existing in some materials when heated from a low-temperature stable phase [40]. Transformation twins form in cooling from the parent phase to the low-symmetry phase, when cooperative atom movements near nucleating sites take place in two or more ways. The motion of the atoms can be presented by a homogeneous deformation matrix added by a set of shear waves called shuffles, which together form the correspondence variants [1].

In certain single crystal metals (e.g., BCC) twinning occurs under increasing stress in the elastic region before the plastic deformation by slip, whereas in other metals (FCC) twinning does not occur before a certain amount of deformation by slip is reached. Presently it is well accepted that twinning in metals is initiated by pre-existing dislocation configurations which dissociate into multi-layered stacking fault structures forming a twin nucleus [12]. This formation of the twin nuclei when a suitable defect configuration is present is named heterogeneous nucleation, while the presumed formation under the action of an applied stress in a near-perfect crystal is called homogeneous nucleation [41]. Several mechanisms have been proposed for describing the twin nucleation. In FCC structures twinning can be explained based on the glide of Shockley partial dislocations, that is, twinning dislocations with Burgers vector $\bar{b} = \frac{a}{6} < 112 >$, where a is the lattice constant. The Shockley partial dislocations would glide on the successive twin planes and create multi-layered faults that could produce a twin [42].

The immediate twinning in the elastic region before slip occurs typically by fast generation of twinned regions and results in sudden load drops of the stress-strain curve [41]. The macroscopic shape change of the material in mechanical twinning is exactly simple shear [40]. The tendency of a

material to deform by twinning or by slip varies widely with, e.g., chemical composition and temperature.

In the materials which exhibit mechanical twinning, it is preferred at low temperatures in comparison to slip. Twinning may occur immediately from the parent phase during or after martensite transformation, since it accommodates the stress. The martensite transformation from the parent phase by stress is called the stress induced MT. Mechanical twinning may occur entirely in the martensite phase, as the relative amounts of the correspondence variants then change. In this type of mechanical twinning, twin boundaries (i.e., twin planes between variants [43]) move as the preferred variants grow at the expense of other variants - this is also called detwinning or the rearrangement of martensite variants [43]. The extent of deformation by twinning in a martensite single crystal depends on the relation of the lattice parameters. In a tetragonal lattice the maximum degree of deformation by twinning is $\epsilon_0 = (1 - c/a)$, when the lattice is changed from one single variant state to another. The deformation principle by the moving twin boundaries is presented in Publication I.

In the classical martensite theory, twins of the centrosymmetric lattice structures are classified to type I (reflection in the twin plane K_1), type II (180 $^\circ$ rotation about twinning shear direction η_1), or compound (mirror) twins [44]. In Ni-Mn-Ga, the observed twins are of the compound twin type, but they have an internally twinned superstructure [33]. Because of the mirror symmetry between the twin and the parent at K_1, there is a change of the atomic positions at the adjacent planes due to the discontinuous lattice. Despite the Wechsler-Lieberman-Read definitions of the lattice correspondence of the variants in the atomic scale [1], there exists an energy barrier ΔE_0 in relation to the surrounding atoms, and the twin boundary thickness l is thus finite as the atomic order reaches to the mesoscopic scale. Barsch and Krumhansl [45] state that by the energy approach the twin boundary thickness l may be calculated by the localized strain energy and the energy barrier as:

$$l = \sqrt{\frac{E(\Delta u)^2}{\Delta E_0}} \tag{1.1}$$

where Δu is the lattice displacement over l and E is modulus. E.g., in ferroelastic tetragonal In-Tl the twin boundary thickness l is suggested to be several atomic layers. In the mesoscale and atomic levels the issue of prediction of the critical stress τ_{crit} (twinning stress), at which a twin initiates in FCC metals, can be approached by the generalized planar stacking

fault energy (GPSF). Kibey *et al.* [42] suggest that τ_{crit} is dependent on the GPSF, but it is influenced by both the intrinsic stacking fault energy and in the nucleation stage by the unstable twin stacking fault energy.

For Ni-Mn-Ga martensites, exact values for the twin boundary thickness have not been reported so far. The hierarchical nature of twins implies that twins of different scales exist in Ni-Mn-Ga alloys.

1.1.3 Twinning systems

Mechanical twinning is characterized by the twinning plane $\{hkl\}$ and the direction of shear, i.e. direction of displacement $< uvw >$ [46]. The twin interface depends on the lattice-invariant plane called the habit plane H. In the simple case of primary twinning (i.e., in the absence of internal twins), H coincides with the twinning plane. In addition to the twinning plane, there exists another invariant plane, which is rotated as a result of the twinning shear [47]. This plane is called the conjugate twinning plane, and its intersection with the twinning plane is the conjugate direction. In the commonly used sign convention by Bilby and Crocker [48], the twinning plane is denoted by K_1, the conjugate plane by K_2, the twinning shear direction by η_1 and the conjugate direction by η_2 as shown in Figure 1.1. The plane of shear has previously been denoted by S, but more recently it is common to use the symbol P as in [41]. The magnitude of the twinning shear is s_t. As shown in Figure 1.1, η_1 is defined by the intersection of K_1 and P, whereas η_2 is similarly defined by K_2 and P.

In some martensite types (also in Ni-Mn-Ga) there exist internal twins, which are secondary twins within the primary twins. The habit plane of the secondary twin forms during the primary twinning, and its prototype is the conjugate twin plane. The twinning elements of the secondary twins are η_1', η_2', K_1', K_2' and s_t [49].

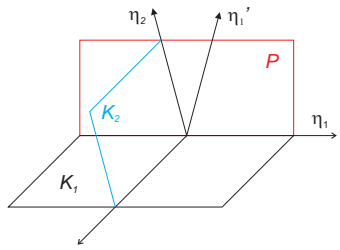

Figure 1.1: The four twinning elements, including the twinning plane K_1 and the plane of shear P presented schematically [41].

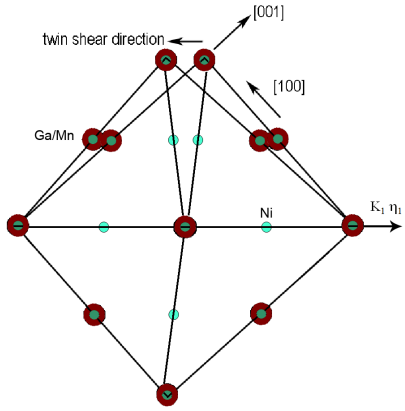

Figure 1.2: A schematic projection of twinning in Ni-Mn-Ga 10M martensite showing the shift of the atomic positions (courtesy of Dr. Y. Ge, Aalto University, published with permission).

Table 1.1: Twinning systems of some lattice types [41, 46, 50, 51].

Lattice type	Twinning plane K_1	Twinning shear direction η_1	Conjugate plane K_2	Conjugate shear direction η_2	Displacement plane P	Example
FCC	$\{111\}$	$< 11\bar{2} >$	$\{11\bar{1}\}$	<112>	$\{110\}$	Ag, Cu
BCC	$\{112\}$	$< \bar{1}\bar{1}1 >$	$\{11\bar{2}\}$	<111>	$\{110\}$	α-Fe
HCP	$\{10\bar{1}2\}$	$< 10\bar{1}1 >$	$\{10\bar{1}\bar{2}\}$	<10$\bar{1}$1>	$\{1\bar{2}10\}$	Cd, Zn
10M (Fmmm)	$\{101\}_C$	$< 10\bar{1} >$	$\{\bar{1}01\}$	<101>	$\{\bar{1}00\}$	Ni-Mn-Ga
NM (I4/mmm)	$\{112\}_M$	$< 11\bar{1} >$	$\{11\bar{2}\}$	<111>	$\{1\bar{1}0\}$	Ni-Mn-Ga

A particular twinning mode is fixed by a pair of K_2 and η_2, but usually twinning mode is expressed by K_1 and η_1. The possible twinning modes are specific for each type of crystal lattice. The conjugate mode has the same P and magnitude of shear, but the twinning planes and directions are interchanged. Some twinning systems are presented in Table 1.1, where also the mainly tetragonal Ni-Mn-Ga martensite structure (10M) is shown. Two coordinate system notations of the 10M Ni-Mn-Ga are mentioned separately, *Fmmm* referring to the parent phase (subscript index C) and *I4/mmm* to martensite phase (M) coordinates. A projection of the twinning in the 10M lattice normal to plane of shear *P* is shown in Figure 1.2. In this figure, $K_1 = (101)$, $K_2 = (10\bar{1})$, $\eta_1 = [10\bar{1}]$ and $\eta_2 = [101]$, with 10M lattice parameters *a*=5.95 Å and *c*=5.61 Å.

The operative twinning mode has to fulfill the following conditions, according to the Bilby-Crocker theory [41]:

- it has a small shear,
- it requires only simple atomic shuffles,
- it requires only shuffles of small magnitude (if possible), or
- it has shuffle displacements parallel to η_1 if large shuffles are essential.

1.2 Twin boundary motion

1.2.1 Influence of stress

Movement of the twin boundaries in Ni-Mn-Ga martensite under applied mechanical stress leads to a shape change and to the pseudoplastic behavior [52]. Various macroscopic modes of deformation such as shear or elongation are enabled by their motion. A simple schematic presentation of the deformation by twin boundary motion in the 10M martensite single crystal material, with only a single twin boundary is shown in Figure 1.3*a*. As the twin boundary moves, the twin variant 1 (with its short c-axis in [001] direction, shown by the blue arrow) shrinks while the neighboring variant 2 simultaneously grows. In the atomic scale the motion of twin boundary requires shifts of the atomic positions, in such a way as schematically shown in Figure 1.2. In a martensite Ni-Mn-Ga crystal there are various small scale shifts of the different kinds of atoms, i.e., shuffling and de-shuffling taking place in the vicinity of the moving twin boundary as proposed by Han et al. [32]. There have been several detailed mechanisms proposed for the motion of single crystal twin boundaries under the influence of stress. The motion of the twin boundary has been proposed to occur by the action of glissile Shockley partial dislocations [41] or by twinning disconnections and disclinations [53]. Despite the movement of twin boundaries under stress being simple to verify in the macroscopic scale, the phenomenon related to it have not yet been entirely clarified in the atomic scale. The direction of the applied load determines the direction of the twin boundary movement (in the limits of ϵ_0), resulting e.g. in contraction or elongation of the material. However, in practice there are

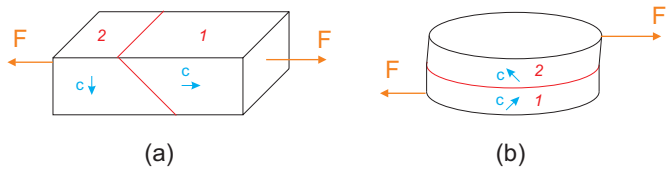

Figure 1.3: Elongation (a) and shear deformation (b) by twinning in the single crystal 10M Ni-Mn-Ga (schematic). The *c*-axis of the variants 1 and 2 are shown by blue arrows. The load F causes the twin boundary trace on the surface (red) to move, as the variant 1 reorientates into variant 2. The twinning angle causes a small tilt of the surface at the twin boundary. The direction of F is assumed to be on the plane P in (b).

often many parallel twin boundaries in the material in the direction set by K_1, and the macroscopic deformation is a result of their combined motion. The twin boundaries may nucleate or annihilate during the deformation if it is energetically favorable. In Figure 1.3*b* the principle of twinning shear deformation is shown, when the flat surfaces of a disc specimen are cut along the 101 planes, and the shear load F is then applied in the plane of the *a* and *b* axes. In this case, the trace of the twin variant boundary is parallel to the flat surfaces, and in Figure 1.3*b* the single twin boundary moves up as the forward shear deformation continues.

The deformation of the material by the twin boundary motion is limited by the crystallographic geometry and when the single variant state is obtained. Outside of the single variant regime, the material cannot be deformed by this mechanism. In a single variant state, a second twin variant in a suitable orientation must nucleate before twinning deformation is possible. In practical measurements by mechanical compression in the [100] and [001] directions, the maximum obtained strain is slightly lower than the lattice-parameter-dependent ϵ_0. In [52] the obtained strain value was about 7 % smaller than the lattice-parameter dependent value, which was determined from the lattice parameters established by X-ray diffraction. In the high quality single crystal, the strain reaches ϵ_0, as is shown in Publication II. In the Ni-Mn-Ga 10 M single crystal martensite, the twin boundary motion begins with a significantly lower axial stress level than what is needed for plastic deformation by slip. When the applied magnetic field is not considered, a sufficient component of shear stress τ in the twinning shear direction, or sufficient resolved shear stress along K_1 in uniaxial compression, is necessary for the twin boundary motion to

occur. When shear stress is applied, the average stress needed for twinning is twinning shear stress τ_t. In uniaxial loading, the resolved shear stress level τ_r for slip may be estimated for example by the Schmidt factor [46, 54]. However, Christian states in his comprehensive review [41] that this approach usually cannot be applied to twinning, as there is large scatter in the measured twinning stresses. The stress-strain curve for the $10M$ Ni-Mn-Ga single crystal usually shows a plateau as the deformation occurs by twin boundary motion. This is followed by a clear and rapid steepening after the twins are fully reoriented. The uniaxial stress value connected to this plateau is generally called the twinning stress σ_{tw}, and describes the resistance to the movement of the twin boundaries. The stress at the start of the plateau σ_{start} is often slightly lower than the stress at the end of the plateau σ_{finish}. A commonly used way for defining the twinning stress is the mean engineering stress of the plateau (i.e., averaging the serrations by a tangent), corresponding to 50 % of the twin variant reorientation. In the case of the 10M material this approximates to 3 % strain. σ_{tw}, σ_{start}, σ_{finish} and the corresponding shear stress values are measurable properties which describe the resistance of twin mobility in martensite. When twin mobility in a crystal is high, these stress values should be low. The strain of the plateau describes the extent of twinning in the crystal, especially when starting from the single variant state. If twin boundaries are not mobile in the entire crystal, the strain remains lower than ϵ_0.

The recent development of the single crystal quality by the material manufacturers has decreased the twinning stress remarkably. The uniaxial twinning stress level of the 10M Ni-Mn-Ga has reduced from a few MPa [55, 56] to σ_{tw}=$0.05MPa$ [57]. Despite the objection in [41], the twinning stress is a crucial material property for the Ni-Mn-Ga alloys. Since it describes the behavior of the material and dictates its performance in several applications [58], it is a central measure of crystal quality and performance.

In addition to the one presented above, twinning stress has been measured in several ways. The most common way for 10M specimens is the uniaxial compression of the pre-oriented sample with the short crystallographic lattice direction transversal to the direction of compression. Some methods of measuring the twinning stress of Ni-Mn-Ga are presented in [59]. Values for the shear stress required for twinning plane movement τ_{req} in various Ni-Mn-Ga alloys are reported by Kakeshita and Fukuda

[60]. For the stoichiometric Ni_2MnGa 10M the minimum value is τ_{req} = 0.5 MPa at T = 160 K, for the non-stoichiometric 14M the min. τ_{req} = 0.8 MPa at T = 300 K, and for NM the min. τ_{req} = 7 MPa at 300 K. Young's modulus E for the $10M$ martensite Ni-Mn-Ga is about 10 GPa, when determined from the stress-strain-curve [61]. Recently, a value of E = 2.2 GPa has been reported by Müllner and King [49] in the elastic regime before the onset of twinning. In the measurements of the elastic constants by the ultrasonic method, the austenite parent phase had C' elastic modulus of about 2.5 GPa and the martensite had C' of about 9 GPa which, when cooled further, dropped to about 4 GPa by the proposed intermartensitic transformation [56].

It has been suggested [62] that surface stresses are important for the successful performance of the MSM alloy. It has been long known, as reported in e.g. [63], that the residual surface stresses, such as the stresses arising from the mechanical grinding, will easily prevent the motion of twin boundaries. Here, the practical solution has been the electropolishing of the specimen surfaces, which reduces the possible surface stresses and thus, enhances the twin boundary motion.

1.2.2 Influence of temperature

The lattice distortion *(1-(c/a))* of 10M martensitic $Ni_{49.0}Mn_{29.6}Ga_{21.4}$ unit cell decreases almost linearly with increasing temperature, as was shown with X-ray diffraction by Glavatska *et al.* [64]. When considering the twin boundary mobility, the decreasing stress needed to move a boundary between variants with decreasing lattice distortions can be expected, since the associated shifting distances of the inter-atomic positions also decrease. This explains the decreasing MFIS and the decreasing critical field for twin boundary activation in 10M Ni-Mn-Ga martensite when the temperature increases [64].

Meyers has gathered several experimental results of twinning stress [65], and concludes that the twinning shear stress τ_t of many metals (Fe, Ag, Cu-20%Zn and others) are in a regime from 50 to 400 MPa. He also states that the critical twinning stress does not strongly depend on temperature, but admits that diverging results exist.

Twinning stress of Ni-Mn-Ga martensite increases when temperature decreases [55, 66]. Kokorin *et al.* found that the TA_2 phonon condensation causes anomalies in the mechanical properties when approaching the MT,

and the material exhibits a premartensitic phase [67]. Thermal phonons were suggested to promote the reorientation of 10M Ni-Mn-Ga martensite under magnetic field [68, 66].

Thermo-mechanical training decreases the onset stress needed for the martensite variant reorientation (Ullakko *et al.* [69]). In the thermally formed self-accommodated martensite the orientations of the martensite variants are usually random. Thermo-mechanical treatment may be applied in order to obtain a variant structure with a desired texture. When the material is stressed during cooling over the MT regime, the low-symmetry martensite phase orientates to accommodate the stress in such a way that a predominant variant is formed. For the 10M tetragonal martensite with (c/a)=0.94 a compressive stress is more applicable, while in the NM martensite with (c/a)>1 tensile stress is more effective. However, in the cyclic experiments a preceding thermo-mechanical treatment over the MT regime reduces the fatigue life of Ni-Mn-Ga, while a mechanical training in the martensite phase provides better performance [70].

Accommodation and reorientation of the variants takes place in the martensite regime, when the twinning stress of the material is not too high. Here, the unfavorable variants vanish by reorientation during a few mechanical straining cycles, and the twinning stress reduces together with the smoothening stress-strain curve, as in [71]. In a material which is possible to train in this way, the macroscopic onset of twin boundary motion and the twinning stress of the entire material decreases. In a material with only favorably oriented variants, further training does not reduce the twinning stress. However, some time-dependency of magnetic field induced strain at a constant temperature has been reported, when the constant field and stress is applied for several hundred seconds [72].

1.2.3 Influence of structure

In a randomly oriented martensite material, there may be twin variants of all possible twinning planes present. In a ferromagnetic martensitic alloy such as Ni-Mn-Ga with many differently oriented variants, a predominant variant state may be created with mechanical training, magnetic field [70] or a combination of them [71]. This applies to the macroscopic twins though referring to the hierarchical twinning concept, there may still be internal twins with different orientation and appearance in the *mainly* single variant state [73]. In practice, magneto-mechanical train-

ing is usually necessary in order to obtain mobile enough twin boundaries, e.g., for the MSM effect to appear. In a sample where only the preferably oriented martensite variants are present [Publication I], the twin boundaries move at a relatively low applied stress - or by a low magnetic switching field H_{sw} in a MSM alloy. The variant state is found to have a significant influence on the onset stress of the twin boundary motion [Publication II]. The twin boundary motion in a *mainly* single variant state sample starts with a significantly higher stress than in a sample with readily existing twin boundaries. A probable explanation for this is that the nucleation of a twin requires higher stress than for the motion of twin boundary; this behavior is also observed in several other metals [65].

In a polycrystalline material the grain boundaries form incoherent interfaces in the crystal, through which the twins cannot easily penetrate. Thus the grain boundaries reduce the mobility of twin boundaries, and the onset stress of twin boundary motion in textured polycrystalline Ni-Mn-Ga is significantly higher than that of the single crystals [74]. Also, the obtainable strain is low and the material behaves more brittle [75]. Usually, the level of twinning stress is too high to obtain MFIS, but with adequate training, a MFIS of 0.5 % has been reached [75]. The brittleness has been partially reduced by hot rolling [76] or by controlled porosity [77]. In the latter case also a repeatable MFIS of 0.115 % was detected. In addition to the grain boundaries, small angle boundaries, and cell boundaries are expected to reduce the twin mobility in a single crystal, but these issues remain to be quantified.

1.2.4 Influence of crystal imperfections and impurities

Crystal imperfections and impurities are known to reduce the mobility of magnetic domain boundaries (generally utilized in hard magnetic materials), and the mobility of dislocations (pinning effect and increase of friction the stress σ_{fr} at dynamic loading [78]). Based on the presented models of the twin boundary nucleation and motion by the twinning dislocations or disclinations [49], a similar hindering effect could be expected for twin boundaries. Marioni *et al.* [79] proposed that the stochastic motion of twin boundaries is a result of the obstacles with varying pinning effect at various positions in the material. Recent experimental results show that reduction of impurities and imperfections improves the mobility of twin boundaries and decreases the twinning stress [57]. In the Ni-

Mn-Ga alloys with relatively low twinning stress, the effective impurity levels are obviously small, although not yet published, and this reduction has required consistent work over several years by the manufacturer. The improvement of the crystal quality was found to enhance the mobility of twin boundaries also in [80].

Several models have been developed for describing the twin boundary motion of MSM materials under the influence of applied stress and magnetic field such as those by Likhachev *et al.* [81], O'Handley [82], Heczko *et al.* [83] and Gauthier *et al.* [84]. Due to the use of generalizations such as mean magnetic field they do not take into account the non-uniform distribution of defects in the material, but their influence is included in the hysteresis or twinning stress parameter. Influence of defects is taken into account in the micromagnetic modeling approach by Paul *et al.* [85]. Their study presents a simplified model based on the magnetic and strain energy equilibrium states for the moving twin boundary. Its movement depends on the stress field of the defect and the energy originated by the external magnetic field. The normalized components of the magnetic field energy h and the strain energy s (originating from the defect) are calculated by normalizing them in respect to the anisotropy energy. The twin boundary is to move, if $h > 1$ and $s < 1$. If s>1, then the twin boundary will not move beyond the defect. L'vov *et al.* state that the positions of crystal defects reconfigure in the martensitic transformation and in variant rearrangement, which contributes to aging. They proposed a slowly varying order parameter, according to the symmetry-conforming theory, for modeling the aging of Ni-Mn-Ga martensite [86].

Typical impurities found in Ni-Mn-Ga materials are sulfides [87] and oxides Publication V, [88]]. In [87], Richard *et al.* state that a sufficient amount of sulfide inclusions prevent the twin boundary motion. In their experiments they used a sublimation process on a Ta-based substrate in order to purify Mn prior to crystallization. The main impurities in the Ni-Mn-Ga alloy were Ta, Ti and S. The existing Ta inclusions allowed the twin boundary motion but they were found to generate cracks when the material was cycled. Ti-inclusions of 5-20 nm acted as pinning sites for twin boundaries, but their pinning effect was possible to overcome by a sufficient magnetic field.

1.3 Magnetic field induced twin boundary motion

1.3.1 Influence of magnetic field

Magnetic field induced twin boundary motion was first reported by Ullakko *et al.* with a magnetic field induced strain (MFIS) of 0.2 % in Ni_2MnGa [89]. The high magnetocrystalline anisotropy of the ferromagnetic twinned martensite in this material made the twin structure to reorient due to the applied external field, simultaneously changing the shape of the material, since the twinning stress was low enough to allow the twin boundary motion. Measured MFIS values reported for some Ni-Mn-Ga alloys are presented in Table 1.2.

In the MSM material, the preferred direction of magnetization changes in the neighboring twin, thus, the application of a magnetic field results in a difference in the Zeeman energy $\mu_0 \mathbf{M_S H}$ across the twin boundary [95]. This energy difference imposes a pressure on the twin boundary, and eventually forces it to move. Saturation magnetization, magnetic anisotropy, and the coercive field of Ni-Mn-Ga are all strongly temperature dependent [43, 96, 97, 98]. They also depend on the chemical composition together with the Curie temperature. A magnetization curve for 10M $Ni_{50.5}Mn_{28.0}Ga_{21.5}$ at 300 K is shown in Figure 1.4. The sample has been pre-oriented by applying a 1 T magnetic field at the [001] direction, and then at the [100] direction. The abrupt increase of magnetization, due to the reorientation of the twin variants by the field occurs at about $2.7 \cdot 10^8$ A/m, as shown in details in the inset. The measured magnetic saturation at 300 K is M_S=75 emu/g. The temperature dependency of magnetization

Table 1.2: MFIS (magnetic field induced strain) values for some Ni-Mn-Ga alloys.

Composition (at-%)	Martensite type	MFIS	Reference
$Ni_{50}Mn_{25}Ga_{25}$	10M	0.002	Ullakko *et al.* [89]
$Ni_{48}Mn_{31}Ga_{21}$	10M	0.051	Söderberg *et al.* [90]
$Ni_{49.8}Mn_{28.5}Ga_{21.7}$	10M	0.06	Murray *et al.* [91]
$Ni_{50.7}Mn_{28.4}Ga_{20.9}$	10M	0.061	Heczko *et al.* [92]
$Ni_{48.8}Mn_{29.7}Ga_{21.5}$	14M	0.095	Sozinov *et al.* [93]
$Ni_{53.1}Mn_{26.6}Ga_{20.3}$	NM	0.017	Chernenko *et al.* [94]

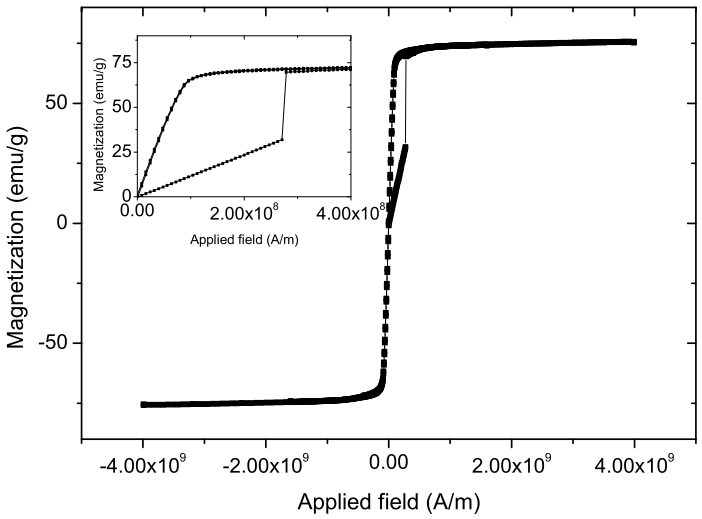

Figure 1.4: Magnetization curve of $Ni_{50.5}Mn_{28.0}Ga_{21.5}$ at 300 K. The inset shows in detail the abrupt change of magnetization due to MSM effect.

at the field of $H_{appl} = 15.9 \cdot 10^6 A/m$ is shown for the range of 4 to 400 K in Figure 1.5. The MT and the reverse transformations, as well as the Curie temperature are indicated clearly by the changes of the magnetization.

1.3.2 Criteria for twin boundary motion in magnetic field

In their model Likhachev *et al.* [99] have stated an equilibrium condition for the MSM effect, namely that the magnetic-field-induced stress has to equal the sum of the internal mechanical stress (at H_{appl}=0, i.e. the twinning-onset stress) and the possible external compressive stress:

$$\sigma_{mag}(h) = \sigma_{mech}(\epsilon) + \sigma_{ext} \tag{1.2}$$

The obvious criterion for the twin boundaries to move by magnetic field is that σ_{mag} is sufficiently large enough to overcome the equilibrium state of Equation 1.2. The magnetic field induced stress is calculated by Equation 1.3:

$$\sigma_{mag}(h) = \frac{1}{\epsilon_0} \int_0^h (m_a(h) - m_t(h))\, \mathrm{d}h, \tag{1.3}$$

where the m_a is the magnetization of the axial and m_t is the magnetization of the transverse twin variant. In a later publication [81] Likhachev concludes that the higher limit for σ_{mag} (when $h \to \infty$) is exactly the same as the uniaxial magnetic anisotropy K_U of the material.

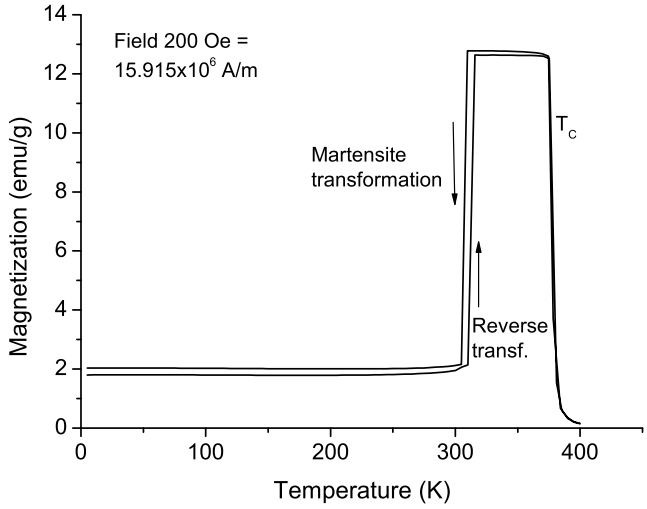

Figure 1.5: Magnetization as a function of temperature for $Ni_{50.5}Mn_{28.0}Ga_{21.5}$ at $H_{appl} = 15.9 \cdot 10^6 A/m$.

Okamoto *et al.* [54, 43] have measured the magnetocrystalline anisotropy constants K_U of 10M, 14M and NM martensites as a function of temperature and showed that they all decrease as temperature increases. For the stoichiometric Ni_2MnGa 10M martensite, the highest value for K_U = 430 kJ/m^3 was obtained at the lowest measured temperature 4.2 K [43]. The same authors report also the calculated magnetic induced shear stress τ_{mag} and the mechanical shear stress τ_{req} required for rearrangement of the martensite variant at different temperatures, and found that τ_{req} increases with decreasing temperature in 10M and 14M martensites. The rearrangement of martensite variants by magnetic field occurred when τ_{mag} exceeded τ_{req} regardless of temperature and the structure of martensite [43]. Glavatska *et al.* [100] determined the temperature dependency of the $Ni_{1.99}Mn_{1.14}Ga_{0.87}$ lattice parameters by the neutron diffraction method in 4-354 K temperature range. They reported that both the magnetic field required for moving the twin boundaries and the MFIS value increase with decreasing temperature as the crystal lattice anisotropy becomes larger. The role of the phonons has importance in Ni-Mn-Ga according to the atomistic simulations made by Entel *et al.* [25]. As twinning stress increases when the material is cooled, it eventually prevents the magnetic field induced strain [96]. The increase of τ_{req} with decreasing

temperature provides an explanation for the lower temperature limit for the occurrence of MSM effect. Heczko and Straka studied the twinning stress σ_{tw} and magnetic anisotropy constant K_1 divided by ϵ_0 for the 10M Ni-Mn-Ga, and concluded that when the temperature decreases below 165 K the σ_{tw} will increase above (K_1/ϵ_0), thus preventing the MSM effect [96]. According to these results, the decrease of MFIS and the lower temperature limit for the MSM effect in these materials is due to the increased resistance to twin boundary motion.

1.4 Energy dissipation and damping

The high vibration damping capacity of the shape memory alloys is generally linked to the presence and the hysteretic mobility of the interphase and inter-variant planar interfaces, but recently it has been revealed that the whole defect structure has to be considered, including those in martensite, as explained in the review of this subject by Humbeeck *et al.* [78]. Each type of defect contributes in damping to a different extent. This allows the optimization of the damping capacity of the SMA based on the requirements set by the later use of the material. The concept of twinning stress σ_{tw} of the martensite material (Equation 1.2) comprising of the hysteretic internal friction-like stresses at $H_{appl} = 0$ directly relates the resistance to straining by twin boundary motion to the damping property. The level of internal friction in Ni-Mn-Ga is relatively high, when compared to, e.g., steel [101]. It is possible to evaluate the resistance to the twin boundary motion by studying the vibration damping properties.

Damping in a magnetic field at low frequencies is expected to be mainly due to hysteresis of twin boundary motion, and the dissipated energy in the material is converted to heat, alike in many metals. At high frequencies (of several hundred Hz), eddy currents may appear and enhance damping, especially when a dynamic magnetic field is present. When damping occurs by the twin or phase boundary motion, a sufficient vibration amplitude as well as stress amplitude based on Hooke's law, must be obtained because of the onset stress for the motion of twin boundaries (and for the possible phase boundaries). Strain amplitude of 10^{-5} is given for this threshold in Cu based and Ni-Ti martensites [78]. Since the strain regime of the twin boundary motion ϵ_0 depends on the lattice parameters,

the effective damping regime is limited by this strain. It is in Ni-Mn-Ga approximately 0.06 for 10M, 0.107 for 14M and 0.20 for NM martensites [58, 30], and approximately 0.04 for the martensite phase boundary damping, when considering the shape memory effect of 4.2 % [102]. Internal friction of the stoichiometric Ni_2MnGa has been studied by Kokorin *et al.* below T = 300 K [10], by Wuttig *et al.* [103] below T = 470 K, and for the non-stoichiometric NM $Ni_{54.5}Mn_{21.5}Ga_{24.0}$ and $Ni_{52.1}Mn_{27.3}Ga_{20.6}$ by Gavriljuk *et al.* in the temperature region from 77 to 473 K [104]. However, in the latter amplitudes only up to $\Delta\epsilon_a = 10^{-4}$ were used and the measured damping properties were not exceptionally high. Stress-induced hysteretic restructuring of martensite was found to retard twin boundaries, and internal friction peaks were found at the phase transformation regimes. Amplitudes $\Delta\epsilon_a = 10^{-4}...10^{-3}$ were applied at temperatures between 125 and 470 K for the non-stoichiometric Ni-Mn-Ga by Segui *et al.*, who obtained loss tangent $\tan\delta$ values below 0.25 [105]. Room temperature damping in $Ni_{50}Mn_{33}Ga_{17}$ was studied by Gans *et al.* [106], who obtained values from 0.6 to 1.1 for the loss tangent $\tan\delta$, and the stress onset for twin boundary motion was 1 MPa. Later studies include those of the author *et al.* (Publications III, IV), and Zeng [107]. Zeng *et al.* reported the damping of 10M martensite in the three different lattice directions and the highest value of $\tan\delta$ was found in the a-c configuration. The $\tan\delta$ dropped significantly when the reverse transformation temperature was exceeded.

1.5 Influence of cycling on twin boundary motion

1.5.1 Structural changes

Shape memory alloys may deteriorate after a reasonably short period when strained with thermal cycling over the phase transformation region in order to obtain the two-way shape memory effect. At first, after 15-20 cycles, there occurs stabilization, and later there is often a decrease of strain output and evolution of cracks. For the Ni-Ti based SMAs, some results are collected in [108], where the maximal reported number of cycles before failure is stated to be 10^3 to 10^4 cycles. Thermal shape memory cycling for over 200 cycles conducted by Xiong *et al.* for $Ni_{49.74}Mn_{28.88}Ga_{21.63}$ single crystal caused crack growth, for which the coexistence of multi-

variants of martensite were proposed to be responsible for [109]. When compared to thermally actuated shape memory alloys, the fatigue life of MSM materials actuated in the martensite phase has been shown to be significantly longer: the highest reported number of cycles is $2 \cdot 10^9$ at $\epsilon_a \cong 2\%$ [Publication VI]. The main reason for this difference is the different deformation mechanism. In the conventional SMA the mechanism is based on the phase transformation and temperature change, while MSM materials change their shape in one phase at a constant temperature. In a MSM material, the cyclic deformation is enabled by the alternation of the fractions of the suitably oriented twin variants (f_1 and f_2). This occurs by the motion of the boundaries separating these variants. The correlation of strain and the variant fractions has been verified by neutron diffraction measurements [52].

In the following, cycling of 10M martensite in uniaxial elongation and contraction under strain control is studied. The two martensite variants are the $[100]$ and $[001]$, distinguished by the orientation of their c-axis in the parent phase coordinates. The fraction of variant 1 is denoted by f_1 and that of variant 2 by f_2, with $f_1 + f_2 = 1$. Depending on the cycling strain amplitude $\Delta\epsilon$, fractions change in each cycle by the amount $\pm\Delta f$:

$$\frac{\Delta\epsilon}{\epsilon_0} = \Delta f \tag{1.4}$$

If $f_1 + \Delta f < 1$ and $f_2 - \Delta f > 0$, there exists a region where the crystal can be cycled. When $\Delta f < 0.5$ there exist two parts in the crystal. A *mobile part*, where the twin boundaries are sweeping across and another part(s) where the twins do not move *(static part)*. As a consequence of this, cycling may change the structure of the material only in the former part. In case of a multivariant state, there may be more than one mobile part or static part in the sample, and the sums of the variants in each part corresponds to the total strain obtainable.

It has been proposed that motion of the twin boundary occurs by mutual movement of twinning dislocations or disclinations in the direction of the twinning plane. As suggested by Müllner *et al.* the twinning dislocations would accumulate to produce a pile-up at a pinning point in the lattice [53, 110]. In general, such pinning points are typically impurity atoms or crystal defects with a stress field, such as dislocations or existing cracks. In Ni-Mn-Ga, pinning of the micromagnetic domain walls, as proposed by Paul *et al.* [85] may also impose a local stress concentration

of the lattice. As was explained before, the preferable direction of magnetization changes across the twin boundary, and the domain wall and the twin boundary coincide as shown by Ge *et al.* [111]. Also, the antiphase boundaries may act as pinning points for domains [112]. Growth of the dislocation or disconnection pile-up can eventually introduce a crack, or cause growth of pre-existing cracks.

1.5.2 Development of twinning stress and strain

Observations of the evolution of twin boundary motion in fatigue have been published in previous studies [62, 113, 114]. They are based mainly on the observations of the MFIS, which is actually also on σ_{ext} and σ_{mag}. Crack growth was found to lead to an eventual failure of the specimen in the magneto-mechanical cycling of both 10M [62] and 14M martensite [70, 114]. Sample preparation methods, such as polishing, have been observed to influence greatly the performance of 10M material.

Changes of the MFIS and fatigue life have varied significantly in all of the previous published experiments, and in all reports the MFIS has changed. The reasons for this are not yet clear, thus further studies need to be performed on the influence of fatigue on the twin boundary motion, and the microstructural changes induced by fatigue.

1.6 Aim of the work

The aim of this Thesis is to clarify the role of twin boundary mobility in the performance of Ni-Mn-Ga alloy single crystals, and to investigate the differences in their behavior in monotonic and cyclic straining. The scientific aims are discussed in more detail below:

1. It is reasonable to assume that twin boundary mobility depends on the structural parameters (such as twin variant configuration, amount of crystal defects and degree of crystal homogeneity) and temperature both in monotonic loading and in dynamic loading (also reflected in vibration damping). It can also be assumed that the mobility of twins in the essentially single variant state, when moving twin boundaries do not exist, is lower than in a structure with existing twin boundaries, i.e. in a two-variant state, because of the nucleation barrier of twins.
   Monotonic stress-strain tests and dynamic vibration damping tests are conducted for different crystals, in order to establish dependencies of twin mobility on different crystal structures and temperature.

2. Twinning in 10M martensite occurs by shear on the $\{101\}_C$ twinning planes, and in η_1 = $<10\bar{1}>$ direction. It may be assumed that twin boundary motion in 10M martensite is dependent on deformation mode and may result both from shear deformation or uniaxial deformation, with comparable twinning stresses but different lattice-parameter-dependent twinning strains.
   To conform this the twinning behavior of 10M martensite is investigated by both uniaxial tests and shear tests in the said twinning mode. The mobility of twins and the behavior of the material in the different modes of deformation is studied.

3. Twins of a Ni-Mn-Ga single crystal can be actuated back and forth over a long term and up to a frequency of several hundred Hz and at several per cent strains. However, it is expected that differences in the material structure influence the twin boundary motion in cycling, and twinning fatigue of the crystal results in microstructural changes that influence the twin mobility and the long-term performance of the material.
   To substantiate these hypotheses vibration damping properties of several Ni-Mn-Ga alloys, using strains of up to several per cent, and the

long-term fatigue performance at cycling frequencies up to several hundred Hz are studied.

2 Experimental

2.1 Sample materials

The Ni-Mn-Ga alloy single crystals used in this Thesis were manufactured by Adaptamat Ltd. Finland (alloys $Ni_{49.9}Mn_{28.2}Ga_{21.9}$, $Ni_{50.0}Mn_{28.3}Ga_{21.7}$, $Ni_{50.1}Mn_{27.7}Ga_{22.2}$, $Ni_{50.4}Mn_{28.3}Ga_{21.3}$, $Ni_{50.5}Mn_{28.0}Ga_{21.5}$ and $Ni_{52.3}Mn_{27.4}Ga_{20.3}$) and by Outokumpu Research Inc. Finland (alloys $Ni_{49.0}Mn_{30.0}Ga_{21.0}$, $Ni_{49.7}Mn_{29.1}Ga_{21.2}$, $Ni_{50.1}Mn_{29.0}Ga_{20.9}$, $Ni_{52.3}Mn_{27.4}Ga_{20.3}$ and $Ni_{55.0}Mn_{22.1}Ga_{22.9}$). All crystals were heat treated in vacuum quartz ampoules for structural homogenization (at 1273 K for 48 h) and for atomic ordering (at 1073 K for 72 h). After the determination of the crystal structure and orientation by XRD measurements, samples were cut by electron discharge machining (EDM) and the surfaces were wet ground and electropolished. The chemical compositions were measured by energy dispersive (EDS) or wavelength dispersive X-ray microanalysis (WDS) by the scanning electron microscope SEM LEO-1450 equipped with Oxford Inca software. For specimens $Ni_{49.9}Mn_{28.2}Ga_{21.9}$, $Ni_{50.0}Mn_{28.3}Ga_{21.7}$ and $Ni_{50.1}Mn_{27.7}Ga_{22.2}$, X-ray fluorescence (XRF) analysis method was applied. The chemical compositions and the primary martensite types are presented together with the corresponding references to results in Table 2.1. Despite the disc shaped shear stress test specimen, the samples were of rectangular shape and their sizes and orientations are described in detail in the corresponding Publications I to VI.

2.2 Microstructural characterization and magnetic measurements

Microstructures of the single crystal surfaces were studied by optical microscope (OM: Leica DMRX using polarized light) and by scanning elec-

Table 2.1: Chemical compositions, martensite crystal structures, transformation and Curie temperatures of the test materials. A reference to the related publication is also given.

Ni (at-%)	Mn (at-%)	Ga (at-%)	Martensite crystal structure	M_s (K)	M_f (K)	A_s (K)	A_f (K)	T_C (K)	Related Publication
49.0	30.0	21.0	mixed	311	297	313	320	375	PIII
49.5	29.4	21.1	10M	324.7	324.4	331.8	331.9	374.0	This Thesis
49.7	29.1	21.2	10M	307	300	316	320	372	PIII
49.9	28.4	21.7	10M	309.2	n.a.	n.a.	n.a.	n.a.	PV
49.9	28.2	21.9	10M	314.0	311.5	320.0	321.4	376.3	This Thesis
50.0	28.3	21.7	10M	315	313	318	320	376	PVI
50.1	27.7	22.2	10M	306.8	305.5	310.6	312.4	376.0	PII
50.1	29.0	20.9	10M	311.2	309.0	319.2	321.4	371.9	This Thesis
50.4	28.3	21.3	10M	322.4	322.0	328.3	328.6	372.5	This Thesis
50.5	28.0	21.5	10M	306.8	305.5	310.6	312.4	376.0	PV
52.3	27.4	20.3	NM	407	400	410	418	380	PIII
52.3	27.4	20.3	NM	406	394	409	420	373	PIV
55.0	22.1	22.9	NM	374	367	376	386	377	PIII

tron microscope (SEM LEO 1450). X-ray diffraction (Philips X'Pert MRD Pro with Co K_α radiation) was applied for studying the crystal structures and orientations of the samples. A laboratory made low-field AC magnetic susceptibility measurement system and a differential scanning calorimeter (Linkam DSC 600, temperature range 77...573 K or Shimadzu DSC-50 with range 123...573 K) were used to determine the magnetic transition and phase transformation temperatures of the alloys.

Magnetic properties at room temperature were studied by a laboratory-built vibrating sample magnetometer (VSM). Temperature-dependent magnetic properties were studied by a Quantum Physics MPMS magnetometer with the temperature range from 4.2 to 400 K. Magnetic field induced strain (MFIS) of the MSM samples was measured by subjecting the sample stick to transverse magnetic field of H_{appl} = 1 T in an electromagnet with a suitable sized air gap after which the sample length l_T was measured by a digital caliper. This was repeated after applying a longitudinal

H_{appl} of 1 T, resulting in length l_L. MFIS was then calculated by the following equation:

$$MFIS = \frac{l_T - l_L}{l_L} \tag{2.1}$$

During the studies these thin samples were supported by a paper roll wrapped around to prevent their buckling in the magnet. When the caliper measurements were carried out any excess force to the sample was avoided. Altogether three independent readings of dimension were always taken and their average values were used. A similar method was used for measuring the dimensions of the samples by caliper, e.g. when determining the cross sectional areas for the engineering stress.

In the case of MSM alloys, also the applied switching field measurement may be used to characterize the mobility of twins. When the sample initially contains twins having the easy axis of magnetization non-parallel to the direction of the slowly increasing applied field, the twins are expected to reorient along the field when the magnitude of the applied field reaches a sufficiently high level. In the MSM alloy the initiation of twin reorientation, i.e. when the triggering field to move the inter-variant twin boundaries is exceeded, a sudden increase of magnetization occurs. This triggering field is distinguishable in the *M*-*H*-curve, especially when the curve is compared to the magnetization curve of the sample which does not have such an abrupt change. The (H_{appl}) value where the magnetization starts to increase due to twin boundary motion, is defined as switching field H_{sw}. Based on the model of Likhachev *et al.* [81], if the magnetic anisotropy and permeability are assumed to be the same, the value of H_{sw} correlates with the twinning stress.

The VSM measurements of H_{sw} were made at the vibration frequency of 20 Hz. Special care was taken in the sample holder configuration in order to avoid external stresses, when holding the sample.

2.3 Mechanical and magneto-mechanical measurements

Uniaxial twinning stress σ_{tw} at monotonic loading was determined from the compressive stress-strain curves, which were measured at room temperature by the servo-mechanical tensile test machine Lloyd 1000R using a load cell withe a range of $\pm$20 N range. The displacement was measured by an internal LVDT type sensor of the test machine. A pre-stress

spring assembly was used for eliminating the possible errors induced by the grip and load cell slack. A separate compression measurement with a steel cylinder having a diameter of 38 mm and length of 33 mm was carried out to verify the stiffness of the system. The test system was found to be adequately stiff in the force range used, and the internal displacement sensor of the machine corresponded well with the displacement of the sample. Static twinning stress measurements were conducted at displacement control with a crosshead speed of 1 mm/min. The limit for compressive stress was set at 3 MPa.

Twinning shear stress tests were conducted using the same test machine as for the uniaxial compression tests but equipped with a $\pm$500 N load cell. The sample was mounted in a steel test jig (Figure 2.1) by applying cyanoacrylate glue with an activator. The strength of the selected glue was suitable for the experiment, since the sample could be removed mechanically from the jig without damage, but the bonding was stronger than the stress needed for the twinning shear. This jig included a linear bearing track, which allowed the shear displacement and prevented essential transverse or rotation displacements, although there was a small amount of slack in the precision bearings. The disc shaped sample with a diameter of 10 mm and thickness of 5 mm is also shown in Figure 2.1a. The strain rate used was $3.3 \cdot 10^{-3} s^{-1}$, and the maximum shear stress was limited to approximately 2 MPa. In all the experiments stresses were calculated as engineering stress and the strain as engineering strain.

Vibration damping properties were studied as a function of temperature by applying two different dynamical mechanical analysis (DMA) systems. T&A Q800 was used in Publication IV and Perkin Elmer DMA-7 in Publication III. In the T&A system the sample can be loaded in two directions, e.g. to impose tensile and compressive linear loading, or alternatively bending back and forth when used in the single cantilever mode. The single cantilever configuration was used for the measurements in the T&A system. The Perkin Elmer device was capable of loading the specimen in only one direction, e.g. bending upwards, while the returning force was created mainly by the weight of the loading members and the elasticity of the sample. It operates under the three point bending (3pb) mode. Both used systems have temperature controlled test chambers and programmable controls as well as data acquisition. Sinusoidal waveform was used for loading the samples. The strain and stress at the single cantilever and 3pb modes, corresponding to the maximum values at the

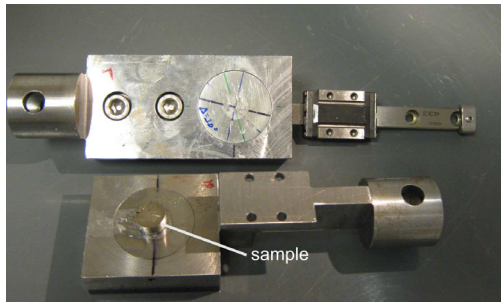

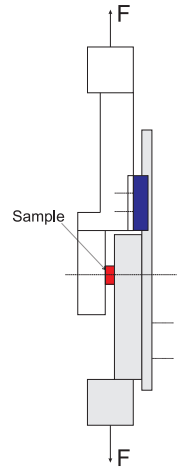

(a) (b)

Figure 2.1: (a): The shear straining test jig with the two parts disassembled. The sample is attached to the lower part. (b): The operating principle of the shear jig. Either compressive or tensile load F can be applied, resulting respectively in reverse or forward shear.

bending beam type sample surface, were calculated by the DMA system.

Magneto-mechanical cycling of the MSM material is based on the repeated magnetic field induced straining and reverse mechanical loading. This kind of actuation principle is commonly used in actuators, mainly due to its relatively simple realization, e.g. [84, 113, 115, 116, 117]. Thus, it is important to study magneto-mechanical cycling of the MSM material and the effects of twin boundary motion in the long–term cycling. In the test system used, a magnetic field was applied in transverse direction to the stick sample, to elongate it. Contraction of the sample was induced by the force of a pre-stress spring, when the magnetic field was reduced. This mechanical loading system ultimately reduces the maximum stroke of the actuator so that in practice it does not achieve the theoretical maximum lattice-dependent strain value. Magneto-mechanical fatigue testing was performed by a specially built actuator-like testing rig, including a non-magnetic sample holder, electromagnetic circuit, and a pre-stress spring for the returning force (Figure 2.2).

The magnetic field was controlled by the applied sinusoidal coil current, regulated by the specifically programmed control software. The frequency was limited to 30 Hz in order to avoid excess heating. Temperature was observed by a thermocouple near the static end of the stick, and the sys-

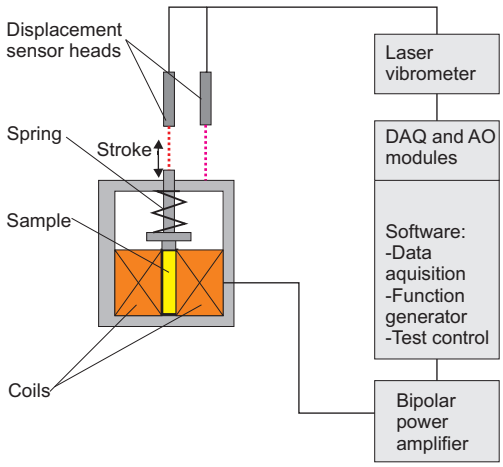

Figure 2.2: The magneto-mechanical cycling test system (schematic).

tem was air cooled. The relative strain of the MSM specimen was calculated by dividing the output stroke of the test jig by the length of the specimen in the axial [001] single variant state (i.e., the short state). Before both the magneto-mechanical tests and the mechanical fatigue tests in Publications V and VI, the rectangular stick samples were magneto-mechanically trained to settle their structure to the two-variant state so that all the twins had their c-axis in the longitudinal direction of the sample or in the transversal (normal to the wider side face) direction of the sample. The amount of individual variants as well as the number of the corresponding twin boundaries varied between the samples and during the tests, as the appearance and disappearance of the variants depends, e.g., on the state of the martensite material and the loading conditions.

When the specimen is installed to the magneto-mechanical test rig, it is first placed in the groove of the sample holder plate made of brass. Then the plate and the sample are together inserted into the air gap of the magnetic circuit. Here the distance from the sample to the surfaces of the magnetic circuit is about 0.3 mm in maximum. The air gap between the sample and the magnetic circuit has to be small in order to allow a strong enough magnetic field to be subjected to the sample. Therefore alignment of the samples is of great importance in avoiding mechanical friction and wear, because the magnetic circuit and the sample holder are static and the sample is moving in respect to them.

When strained, the stress of the MSM material is relatively low in the strain regime where the twin boundary motion occurs. Outside of this

regime, i.e. in the single variant state, the stress increases rapidly. It is important to ensure that the sample is not strained beyond the twinning/detwinning regime under strain control, since the resulting high stress would damage the sample. In the magneto-mechanical cycling test no external load is applied to the sample, except the load of the pre-stress spring. The stress of the MSM specimen in this case is limited by the magnetic field induced stress (in the 10M material typically about 3.5 MPa) and by the approximately 1 MPa compressive stress of the pre-stress spring, if the mechanical friction forces and the dynamic mass forces are neglected. In this respect, it may be assumed that the stress during the magneto-mechanical cycling is mainly within -1 to +3.5 MPa. However, in the case of purely mechanical cycling at zero (ambient) magnetic field, the applied external stress is generated by the test system, and the stress is not limited by the intrinsic material properties. Especially when cycling crystals under strain control, the unwanted transient stresses have to be separately considered.

In order to limit the stress transients in the mechanical fatigue test, the sample was prepared and installed to the test rig in a certain manner. Before the start of the test, the sample was settled manually to about 3 % strain, i.e., about half of the theoretical maximum of the lattice dependent maximum strain allowable by the twin boundary motion. When the strain amplitude is limited to the strain regime below approximately 2.5 %, the sample cannot enter the single variant state, which is suspected to be hazardous for the fatigue life.

For the mechanical fatigue experiments at zero (i.e., ambient) magnetic field, a laboratory-made testing rig was used. It was built as a part of the Master's degree [118] supervised by the author. The testing rig is capable of loading the sample at the frequency of several hundred Hz and at several percent strains. The system is programmable and can be run either at displacement control or at load control. The data acquisition system was used to record averaged stress-strain loops at user defined intervals. In addition, a computer program recorded the twinning stress as well as several other parameters. Twinning stress in this case was calculated as half of the difference of the tensile and compressive stress at the zero strain value, corresponding to the initial length of the sample at the start of the experiment. Adjustable displacement limiters were set by the software in addition to the mechanical limiter for the moving axis of the system. These are needed to limit the stroke within the two-variant

state. In this mechanical cycling rig the sample is compressed between the grips from its side surfaces <001> at the stick ends. Consequently, in this region the twins do not reorient because of the compressive stress, and this length is omitted from the measurement length when calculating the strain. In this construction the sample is between the grips free of any contact, so there is no possibility for mechanical friction.

3 Summary of the Results

3.1 Twin boundary motion in magnetic and mechanical monotonic loading

3.1.1 Uniaxial compression and switching field tests

Twinning behavior and its dependence on temperature was studied in Publications II and III. The alloy $Ni_{49.0}Mn_{30.0}Ga_{21.0}$ with an inhomogeneous mixed martensite structure was studied in monotonic uniaxial compression in Publication III. At room temperature the onset of twinning took place with the applied stress of approximately 1.2 MPa, and at the end of the plateau the stress was approximately 3.5 MPa. Both of these stress values decreased as temperature increased to approach A_s. At the same time the maximum twinning strain reduced by about 1 % strain.

The twinning behavior of $Ni_{50.1}Mn_{27.7}Ga_{22.2}$ 10M martensite single crystal in the ambient magnetic field was studied in the essentially single variant state and in the presence of two twin variants at room temperature in Publication II. The sample was prepared so that it had its sides along the {100} crystal planes. The initial variant state was produced to the sample by applied transverse magnetic field before the mechanical loading. The single variant state ([100]) was produced by applying a field of H_{appl}=1 T and the two-variant state ([001] and [100]) with H_{appl}=0.35 T. In the optical microscope the single variant state of the sample appeared to lack the macroscopic twin boundaries, whereas in the two-variant state twin boundaries were visible. Since it is in principle possible that in the former state there exists very thin twins, which are too fine to be detected by the optical microscope, the term *essentially* single variant state is used here. The compressive stress strain curves of Figure 3.1*a* and *b* show that the onset stress needed for twin boundary motion is significantly larger in the essentially single variant state than when even a small amount of secondary variant exists. This variant state dependent behavior of the

material was repeatable, which is shown by the compressive curves.

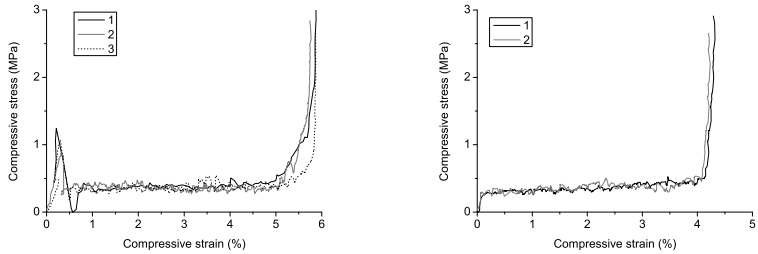

(a) Essentially single variant state. (b) Two-variant state.

Figure 3.1: Compressive stress strain curves of $Ni_{50.1}Mn_{27.7}Ga_{22.2}$ in the essentially single variant state (a) and in the two variant state (b) [Publication II].

To investigate in detail the behavior of the 10M martensite Ni-Mn-Ga single crystals in the different variant states, uniaxial stress was applied to <100> oriented rectangular single crystal specimens at room temperature. The repeated compressive stress-strain curves of $Ni_{50.1}Mn_{29.0}Ga_{20.9}$ material in the zero applied magnetic field and at room temperature are shown in Figure 3.2. Before the experiment, the sample was partly reoriented to the [001] variant state by applying a 1 T magnetic field in alternating angles relative to the sample. This yields different pre-strains corresponding to the different fractions f_2 of secondary variants of type [100]. In the test the twinning stress varies in a saw-tooth-like way as the sample is compressed, which is typical of heterogeneously twinning martensite [41]. In an essentially single variant state ($f_2 = 0$, M1 in Figure 3.2) twin boundary motion starts at σ_{start}=1 MPa, and it continues with gradually increasing stress up to σ_{finish}=1.8 MPa with compressive strain $\epsilon \approx 0.06$, when the entire twin structure is reoriented. With larger amounts of the secondary variant (increasing f_2) the onset stress for twinning appears to be lower starting from 0.6 MPa. In this experiment, at all the variant states, the twin boundary motion takes place in the stress range from 0.6 to 1.9 MPa. The highest stresses for twinning occur for the $f_2 = 0$ state. The difference of the stress levels for the samples in various f_2 initial states is $\sim$0.5–0.6 MPa.

In the compressive stress-strain curves of another type of 10M material $Ni_{50.4}Mn_{28.3}Ga_{21.3}$, there is a large variation in the compressive stress needed to move the twin boundaries (Figure 3.3). When the fraction of the secondary variant is very low ($f_2 = 0$ or $f_2 = 0.09$) detwinning requires

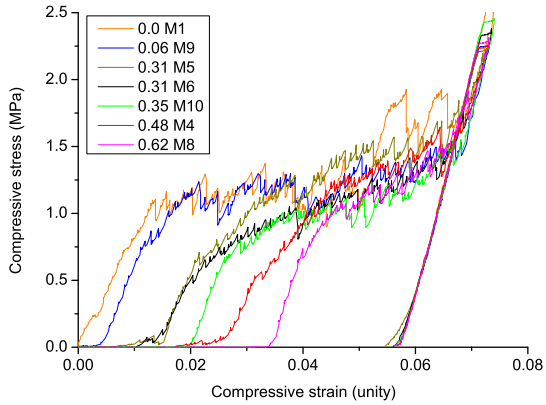

Figure 3.2: Compressive strain-stress curves of $Ni_{50.1}Mn_{29.0}Ga_{20.9}$ at different secondary variant fractions f_2. The numbers at the end of the legend indicate the order in which the compressions were done.

a distinctively high stress, when compared to the stress needed with the larger f_2. In these successive compressive tests at larger fractions of the secondary martensite variant, the twinning stress was in some tests very low, even about 0.05 MPa at $f_2 = 0.35$, but in all cases the twinning stress increased to the level corresponding to $f_2 = 0$ before the maximum strain ϵ_0 was reached.

Thus, depending on the twin variant structure, the stress needed to move the twin boundaries in a sample varies from between 0.05 to above 1.0 MPa. The highest twinning stress was related to the essentially single variant state structure. Furthermore, the boundary requires a continuously increasing stress while moving through the sample (Figure 3.3). This suggests that in addition to the high amount of energy necessary for the nucleation of the secondary variant, as reported in Publication II, in some alloys the twinning stress may remain high while a twin boundary is moving. In these cases, the onset of the twin boundary motion is sudden and instantaneous - in contrast to the smooth and gradual stress onset found for example in $Ni_{50.1}Mn_{29.0}Ga_{20.9}$ (Figure 3.2).

The crystallographic structure of the 10M martensitic specimens $Ni_{50.4}Mn_{28.3}Ga_{21.3}$ and $Ni_{50.1}Mn_{27.7}Ga_{22.2}$ was studied by X-ray diffraction from the thin sides of the rectangular specimens, which were supposed to be oriented along the (010) planes. This surface corresponds to the front surface (the one with the blue arrows) in Figure 1.3*a*. The two

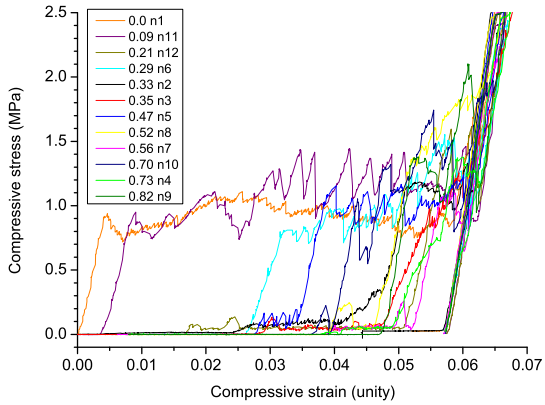

Figure 3.3: Compressive strain-stress curves for $Ni_{50.4}Mn_{28.3}Ga_{21.3}$ at different secondary variant fractions f_2. The numbers at the end of the legend indicate the order in which the compressions were done.

specimens were settled to intermediate lengths, corresponding to multivariant states, by elongating and contracting them gently with the fingers of the hands. The 10M martensite peaks using Co K_α radiation were found as expected near 2Θ=74° (corresponding to (040) or (400)) and 79° (004). This confirmed that the specimens were in a multivariant state. In addition there existed minor peaks near 2Θ=66° and 2Θ=83°, which can be interpreted to be modulation peaks based on the superlattice [119]. The intensities of the peaks were studied as a function of the sample length by manipulating the specimen along its long axis while keeping the rotation and tilt of the XRD goniometer constant, corresponding to the observed peak position. The intensity of the modulation peaks showed more variation in specimen $Ni_{50.1}Mn_{27.7}Ga_{22.2}$ than in the specimen $Ni_{50.4}Mn_{28.3}Ga_{21.3}$. This result suggests that the latter specimen has a more homogeneous crystal structure than the previous specimen, where the modulation is not as evenly distributed.

The macroscopic twin structure of the broad surface of the sample stick $Ni_{50.4}Mn_{28.3}Ga_{21.3}$ was studied by polarizing optical microscopy after the XRD measurement. This surface corresponds to the top surface in Figure 1.3*a*. The microscope revealed the traces of the macroscopic inter-variant boundaries (Figure 3.4). The width of the twins varied, and there existed broader twins than in the $Ni_{50.1}Mn_{27.7}Ga_{22.2}$ sample. The motion of the twin boundaries in the $Ni_{50.4}Mn_{28.3}Ga_{21.3}$ sample was studied by

elongating and contracting it manually after microscopy, where the easily and hard moving twin boundaries were located in the sample at distinct regions. In Figure 3.4*a* the variant boundary at the left side of the marked region was movable with a very low stress below 0.1 MPa until the twin boundary reached the right side of the marked region. Beyond this point the further deformation was not possible at such a low stress, as the part of the sample outside the marked region contained only hard moving boundaries. The more detailed Figure 3.4*b* of the surface shows that the marked twin boundaries on the left side of the marked region are not parallel, but have an angular difference of about 5 °. This is unexpected, since the twins in the single crystal sample are expected to have either the same twinning plane K_1, or to have a larger angular difference, e.g. approximately 45 ° due to having been twinned on separate planes of the same form, such as (101) and $(10\bar{1})$. Figure 3.4*c* details the right side of the region showing that there is a difference of about 0.6 ° in the twin boundaries at the border of the easily moving regions and at the hard moving regions. In addition, the twin boundary separating the easily moving region from the hard moving one has a different structure, as there are two straight twin boundaries emerging from opposite sides of the surface, meeting at a bending point at the angle of approximately 4.5°, forming an obtuse V-shaped interface. It is notable that the motion of the easily moving twin boundaries are limited by this V-shaped interface shown in Figure 3.4*d*, and also by the angularly differing twin boundaries shown in Figure 3.4*b*. Further experiments showed that the locations and the amounts of the hard and easily moving boundaries changed when the sample was trained by successive mechanical bending and uniaxial magneto-mechanical training. However, this behavior did not seem to be easily repeated. The optical microscope also revealed that the density of visible twin variant boundaries in the multivariant state was greater in specimen $Ni_{50.1}Mn_{27.7}Ga_{22.2}$ than in specimen $Ni_{50.4}Mn_{28.3}Ga_{21.3}$, suggesting a more homogeneous crystal structure for the latter specimen.

In addition to the mechanical straining, a method based on the magnetization was also applied in order to study the twin boundary mobility in the single crystal Ni-Mn-Ga material. The results in Publication II showed that the applied switching field H_{sw} onset-value is larger for the sample in the single variant state than for the sample with a reasonable amount of the secondary variant. The magnetic field-induced stress at the onset of twin boundary motion was calculated from the obtained H_{sw} values by

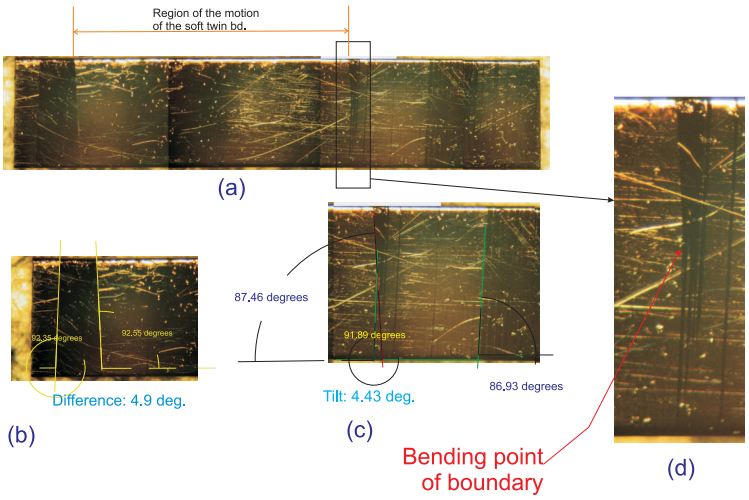

Figure 3.4: Optical micrographs of the twin variant boundaries on sample surface. The angle of the twin boundary in relation to the sample side surface is shown in the inset (*b*) for easily moving boundary and in (*c*) for hard moving boundary. The tilted hard boundary is shown in detail in (*d*).

Equation 1.3. In Figure 3.5 the H_{sw} and magnetic field induced stress is shown together with the measured compressive stress onset values at different secondary variant fractions in the $Ni_{50.1}Mn_{27.7}Ga_{22.2}$ sample.

3.1.2 Shear tests

Shear twinning behavior

Since the macroscopic shape change in twinning of martensite is simple shear, twinning behavior of the single crystal 10M $Ni_{49.9}Mn_{28.2}Ga_{21.9}$ and $Ni_{49.5}Mn_{29.4}Ga_{21.1}$ was studied under shear stress at room temperature. The samples were magneto-mechanically trained before the experiment at room temperature with H_{appl}=1 T field. The disc-shaped samples were sheared at a constant strain rate $\dot{\gamma} = 3.3 \cdot 10^{-3}\ \frac{1}{s}$ to selected directions, forwards and backwards. The experiments are listed in Table 3.1, and their results are presented in detail in the following section.

The shear strain-stress curves of $Ni_{49.9}Mn_{28.2}Ga_{21.9}$ sample S1 along the shear direction [10$\bar{1}$] are presented in Figure 3.6. Both the first and second forward shear curves are shown. The offset of the shear strain scale is not exact, since the original displacement was measured by the internal sensor of the test machine, however, the shear strains calculated

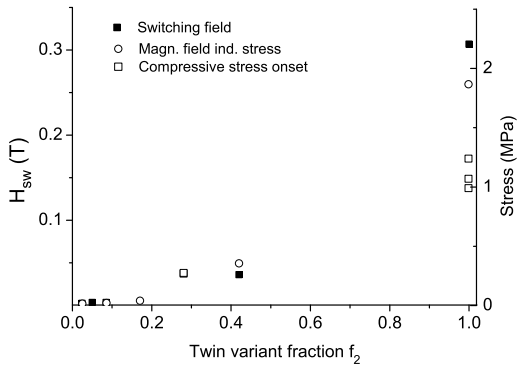

Figure 3.5: H_{sw}, calculated magnetic field induced stress and compressive stress for twin boundary motion at different secondary variant fractions in $Ni_{50.1}Mn_{27.7}Ga_{22.2}$.

with the tangent lines (shown in Figure 3.6) are correct within reasonable accuracy ($\approx \pm 0.02\%$).

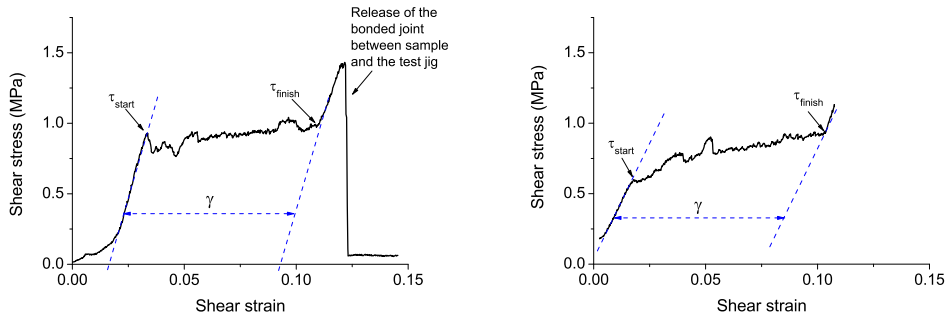

Figure 3.6: Shear stress-strain curves for 10M $Ni_{49.9}Mn_{28.2}Ga_{21.9}$ at room temperature. Curve (a) shows the results of the first and (b) second forward shear test. The points of τ_{start} and τ_{finish} and the shear strain γ are indicated.

Twinning in the first shear test (sample S1) initiated at τ_{start}=0.91 MPa (Figure 3.6a). The shear proceeds with a slightly fluctuating and increasing stress as the twin variants of the sample reorient. At the end of the plateau the shear stress is τ_{finish}=0.97 MPa. The extent of shear in the first shear test was γ=0.076, when determined from the onset of twinning to the end of the plateau. When straining was continued further, the glue between the sample and the jig ruptured off. The sample was then

Table 3.1: Shear test results for the 10M single crystals. The shear load was applied along the [10$\bar{1}$] direction.

Alloy	Sample name	Number of preceding strainings	τ_{start} (MPa)	τ_{finish} (MPa)	τ_t (MPa)	γ
$Ni_{49.9}Mn_{28.2}Ga_{21.9}$	S1	0	0.91	0.97	0.94	0.076
	S1	1	0.60	0.93	0.77	0.085
	S2	1	0.49	0.60	0.55	0.08
$Ni_{49.5}Mn_{29.4}Ga_{21.1}$	SO	0	1.4	1.3	-	0.117
	SO	3	0.41	0.75	0.58	0.111
	SO	10	0.33	0.58	0.46	0.113

re-glued to the jig, and reversely sheared back to its original shape. For the second forward shear experiment (sample S1) τ_{start}=0.60 MPa and τ_{finish}=0.93 MPa were obtained, while the twinning shear was γ=0.085 (Figure 3.6b). The τ_{start} is now clearly lower than in the first straining, and also the τ_{finish} has reduced slightly. The twinning shear stress, calculated as the average value of the plateau is in the first cycle τ_t=0.94 MPa and in the second cycle τ_t=0.77 MPa. For another similarly shaped sample S2, prepared of the same material and having same orientation as S1 (Figure 3.7), the corresponding τ_{start} is 0.49 MPa and τ_{finish} is 0.60 MPa, and γ=0.08 when measured from the forward strain of the second cycle. Correspondingly, τ_t of the second sample is 0.55 MPa. The twinning shear stress results show rather large variation between the different specimens and also the shear stress seems to decrease during the successive straining cycles i.e., the so called training effect typical of compressive tests exists also in shear. The twinning shear γ shows variation between the different specimens and strainings.

Twinning under shear strain in the $\eta_1 = [\bar{1}01]$ direction was also studied with a $Ni_{49.5}Mn_{29.4}Ga_{21.1}$ specimen (SO) having an octagon-shaped cross section (dimensions 8 x 8 x thickness 5 mm^3). On the flat surfaces of this specimen the twins were more easily observable than on the round surface of the disc specimens. According to the manufacturer, crystallization process improvements had been made when producing this material, when compared to the earlier produced test material $Ni_{49.9}Mn_{28.2}Ga_{21.9}$. This suggests that the former material has a higher purity. The shear

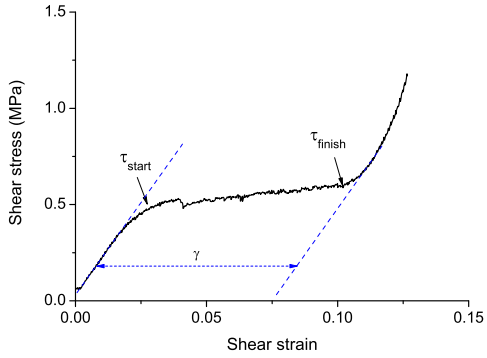

Figure 3.7: Shear stress-strain curve of sample S2 of $Ni_{49.9}Mn_{28.2}Ga_{21.9}$.

stress-strain curve for this material (sample SO) in the electropolished essentially single variant state before significant deformation is shown in Figure 3.8*a* and the curve for the mechanically shear-trained (three times) state is shown in Figure 3.8*b*. In the essentially single variant state without training (Figure 3.8*a*) there is a significant increase of stress (peak), which is abruptly released and then followed by the twinning shear. The shear stress at the peak is 1.42 MPa, with the stress dropping to 0.55 MPa at the beginning of the plateau. The stress increases again gradually with shear strain up to τ_{finish} = 1.33 MPa where the plateau is finished with plateau strain γ = 0.117. This peak diminished with training, as can be seen in the curve of Figure 3.8*b*. The shear strain in the trained state is almost the same as prior to training, but the peak no longer exists. Furthermore, the twinning shear stress has decreased (τ_{start} = 0.41 MPa) and the plateau is now almost horizontal, as τ = 0.50 MPa at as high a strain as γ = 0.10.

The shear stress-strain curves of $Ni_{49.5}Mn_{29.4}Ga_{21.1}$ (Figure 3.8) differ from the $Ni_{49.9}Mn_{28.2}Ga_{21.9}$ curves. The former samples show generally a lower twinning stress level and in the trained state (Figure 3.8)*b*) a larger twinning strain.

With further back and forth shear straining (ten times) the twinning stress of $Ni_{49.5}Mn_{29.4}Ga_{21.1}$ reduced even further as shown in Figure 3.9. Twinning starts now at τ_{start} = 0.33 MPa and then continues with decreasing stress at τ_{min} = 0.23 MPa, and then with increasing stress up to approximately τ_{finish} = 0.58 MPa. When inspected in detail, there is a small starting shear strain starting already at approximately τ = 0.07

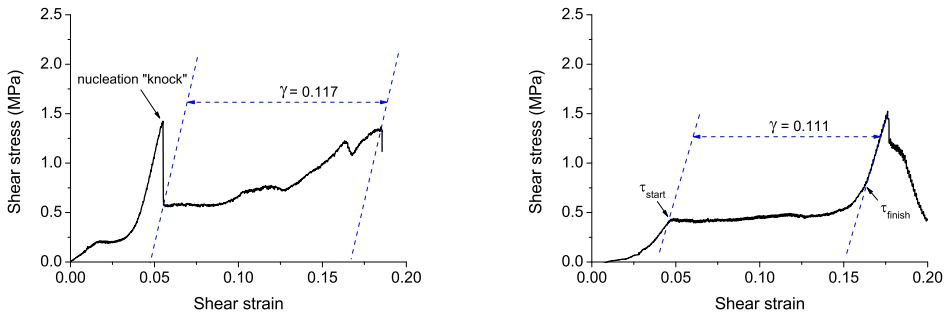

Figure 3.8: Shear stress-strain curves of 10M $Ni_{49.5}Mn_{29.4}Ga_{21.1}$ (sample SO) (a) in the untrained state and (b) in the trained state.

MPa, although the more continuous twinning begins at 0.33 MPa stress. When the small shear strain is included γ is 0.119 and without it γ is 0.113.

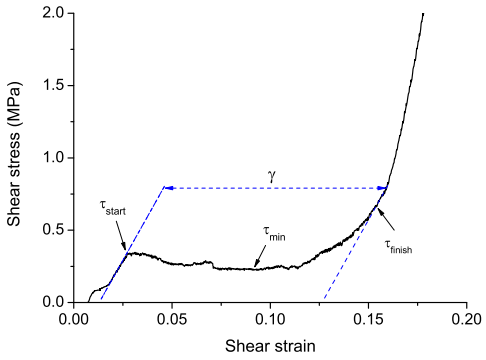

Figure 3.9: Shear stress-strain of 10M $Ni_{49.5}Mn_{29.4}Ga_{21.1}$ at the trained state.

X-ray diffraction investigation

XRD measurement was carried out before the shear test for determining the crystal structure and orientation of the shear specimen S1 $Ni_{49.9}Mn_{28.2}Ga_{21.9}$. The S1 sample was oriented in the (101) direction with a difference of 4°, and its lattice parameters were a = 5.94 Å and c = 5.59 Å. Using these values, the maximum lattice-dependent strain in the shear direction would in the $Ni_{49.9}Mn_{28.2}Ga_{21.9}$ alloy be γ_0=0.12. The ob-

served shear strain values are smaller than the calculated γ_0. According to the plateau strain, about 70 % of the specimen was reoriented by shear twinning in the second cycle of the first sample. The corresponding degree of reorientation of the second specimen was about 67 %.

The 4° orientation difference between the sample disc surface and the (101) twinning plane causes an error of 0.002 to shear strain. The estimated alignment error of gluing the sample to the shear test jig, between the loading direction and η_1 is about $\pm 2°$ in a direction almost perpendicular to the (101) plane. The total error arising from these factors to shear strain is 0.003, which is approximately 3.8 % of the measured γ values.

The (202) XRD pole figure of the specimen S2 after the shear test is presented in Figure 3.10a. The figure confirms that the change of the (202) variants in the shear has been incomplete. Determined by the XRD texture analysis of the pole Figure 3.10a, the intensity after the shear test for the peak corresponding to variant 1 is $I_{V1} = 60.2 \cdot 10^3 cps$ and for variant 2 is $I_{V2} = 170.6 \cdot 10^3 cps$. The corresponding peaks are indicated in Figure 3.10*a* by circles. Assuming that the specimen would have been in the single variant state before the shear test, the XRD peak intensities can be used for calculating the shear strain γ by the following equation:

$$\gamma = \gamma_0 \cdot (1 - \frac{I_{V1}}{I_{V1} + I_{V2}}), \tag{3.1}$$

where γ_0 is as defined above. When γ_0 = 0.12, and I_{V1} and I_{V2} are as above, the value of the shear strain γ = 0.088. The optical image of the side surface of the shear specimen S1 in Figure 3.10*b* shows that the twins are aligned along the loading axis in a similar way to that presented in Figure 1.3*b*. The corresponding image of the shear specimen S2 in Figure 3.10c shows that the twin boundaries in this case have approximately 55° inclined orientation in relation to the loading axis, instead of being aligned parallel to it. However, due to the curvature of the specimen surface, determination of the angle from the optical image is not very accurate. Based on the observed approximate orientation of the variant boundaries in reference to the crystallographic axes of the XRD pole figure, the twins of Figure 3.10*b* are {101} twins and the ones in Figure 3.10*c* are {011} twins. The images were captured after the shear straining while one jig plate was still glued to the specimen and the other plate was sheared off. Scraping off the remaining glue before inspection was not done as it could have deformed the specimen further. Because of this, some glue is visible in Figure 3.10*b*.

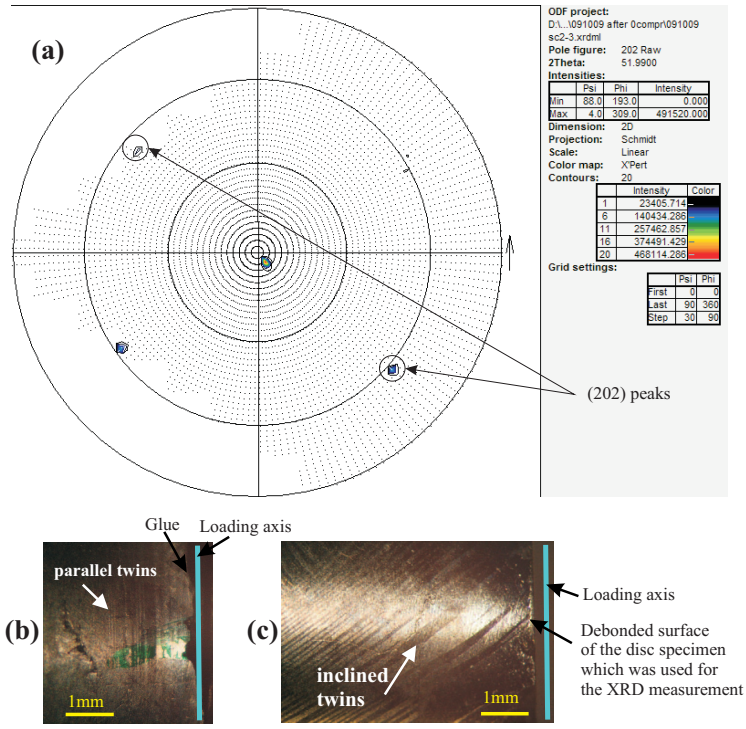

Figure 3.10: (a) (202) XRD pole figure of the second 10M shear specimen $Ni_{49.9}Mn_{28.2}Ga_{21.9}$. (b) An optical image of the curved side surface perpendicular to the loading direction of the first shear specimen. The twins parallel to the loading axis are indicated. (c) A corresponding optical image of the curved side surface of the second specimen showing the twin structure which is inclined in relation to loading axis.

The lattice parameters of the alloy $Ni_{49.5}Mn_{29.4}Ga_{21.1}$, which were also determined by XRD, are a = 5,96 Å and c = 5.58 Å. Using these lattice parameters, the calculated maximum shear strain γ_0 along the $[\bar{1}01]$ direction for this alloy is 0.13. The observed shear strain in the trained state (Figure 3.8)*b*)) is approximately 85 % of the calculated maximum value γ_0. In the further trained state the observed shear strain is approximately 92 % of γ_0.

3.2 Twin boundary motion in dynamic loading

3.2.1 Twinning induced damping

In Publication III the loss tangent $\tan\delta$ is applied to describe the different damping properties as a function of temperature of several Ni-Mn-Ga materials having 10M ($Ni_{49.7}Mn_{29.1}Ga_{21.2}$), NM ($Ni_{52.3}Mn_{27.4}Ga_{20.3}$, $Ni_{55.0}Mn_{22.1}Ga_{22.9}$) or mixed ($Ni_{49.0}Mn_{30.0}Ga_{21.0}$) martensite structures. In all these alloys the $\tan\delta$ is higher in the martensite state than in the parent phase, and the peak values are obtained at the phase transformation regions. In alloys with a NM martensite structure, the $\tan\delta$ increases gradually until the A_s temperature. The high damping state of the (NM martensite) $Ni_{52.3}Mn_{27.4}Ga_{20.3}$ alloy with A_s temperature of 410 K extends to above 400 K. With the samples having a mixed or 10M martensite structure, the highest damping during heating is reached already at 290 K, although the phase transformation peak is approximately at 315 K. Similarly during cooling the highest damping property is found 20 K below the transformation peak. Twinning induced damping was highest in the studied martensites in the 10M martensite $Ni_{49.7}Mn_{29.1}Ga21.2$ ($\tan\delta \approx 0.25$ [Publication II]) and in the NM martensite $Ni_{52.3}Mn_{27.4}Ga_{20.3}$ ($\tan\delta \approx 0.5$ [Publication IV]).

The dynamic modulus measurements of NM $Ni_{52.3}Mn_{27.4}Ga_{20.3}$ alloy in Publication IV show that the modulus in the martensite state is stress amplitude dependent, whereas in the cubic phase region there is no essential dependency on stress. This implies that the primary mechanism of damping in the martensite phase is the hysteretic motion of martensite twin boundaries. The $\tan\delta$ measurements of the same material in Publication III confirm that the loss tangent in the martensite phase is about two decades higher than that in the parent phase. The DMA method was used to study the strain amplitude dependency of the NM $Ni_{52.3}Mn_{27.4}Ga_{20.3}$ in the single cantilever bending mode. The $\tan\delta$ as a function of applied bending strain (as the maximum value on the sample surface) is shown in Figure 3.11. The $\tan\delta$ increases clearly with strain amplitude, which suggests that the damping is induced by the twin boundary motion. The loss tangent of the martensitic material is slightly more temperature dependent and the maximum strain increases with the temperature, which is connected to the decrease of the dynamic modulus with the increasing temperature [Publication III]. When the strain amplitude dependency is

considered, the $\tan\delta$ as a function of applied strain amplitude seems to follow roughly the same levels at different temperatures [Publication III]. All the results shown in Figure 3.11 are clearly in the martensite regime (below A_s = 409 K). Since the total distance that the twin boundaries traveled, i.e., the sum of the distances traveled by many boundaries, in single crystal Ni-Mn-Ga martensite is directly dependent on strain, it is suggested that the damping properties in this martensite depend essentially on the extent of the twin boundary motion.

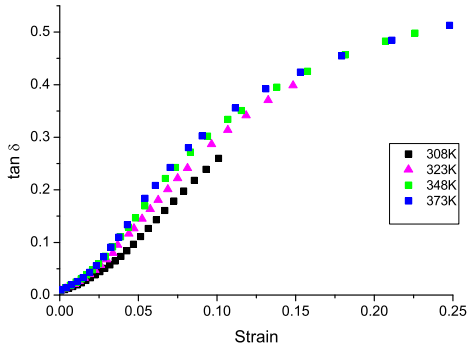

Figure 3.11: The loss tangent ($\tan\delta$) as a function of strain amplitude of $Ni_{52.3}Mn_{27.4}Ga_{20.3}$ at different temperatures in martensite (A_s = 409 K). The measuring frequency was 95 Hz and the measurements were performed in ascending order of temperatures.

3.2.2 Effects of cyclic loading

The practical uses of the twin boundary motion of Ni-Mn-Ga material are presently in the MSM actuators, and in vibration damping. In these applications the twin boundaries are expected to be driven back and forth in numerous cycles by a magnetic field or by applied mechanical stress. It is generally accepted that fatigue causes structural changes in metals. On the other hand, the possible changes in onset of motion and the behavior of the twin boundaries, such as the amplitude dependency of stroke, have an influence on the performance parameters of the material. Therefore, the effects of cycling are crucial to the lifespan and controllability of the material. Thus, it is not enough to study only the effects of the structural properties on twin boundary mobility, but it is important to obtain experimental information of their possible changes in the long-term cycling.

In Publication VI the effects of cyclic loading on the 10M $Ni_{50.0}Mn_{28.3}Ga_{21.7}$ were studied in the mechanical cycling experiments at zero magnetic field (i.e. ambient) at room temperature. In the strain controlled experiments, the twinning stress of one sample measured from the cycling stress-strain loop increased only slightly up to $160 \cdot 10^6$ cycles, after which the sample cracked. Another sample of the same material, when using first load-control and later strain-control, tolerated up to $2 \cdot 10^9$ cycles, while the strain was changing in the range of 0.013 to 0.0217, and the twinning stress varied from 0.44 to 0.71 MPa. Many of the changes in twinning stress are associated with an abrupt change of strain or applied stress. E.g. in Figure 3.12 at the number of cycles $N = 188 \cdot 10^6$ there is observed a decrease of the twinning stress co-incidental with decreasing of both applied external stress and strain. A gradual increase of the applied stress was found after several tens of millions of cycles, which is needed in order to retain the same strain level in the cycling. This phenomenon was related to the increased slope of the stress-strain-loop as the cycling test proceeded. It is observed as the steepened slope of the stress-strain loops in Publication VI.

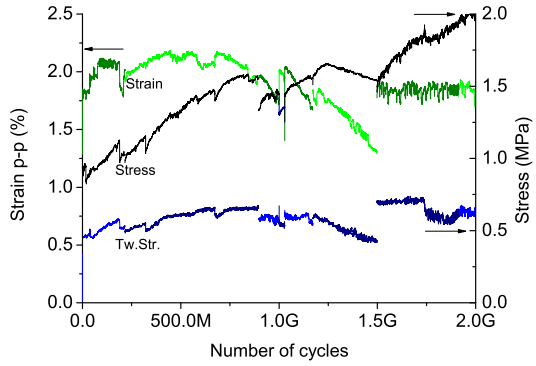

Figure 3.12: Applied stress, strain and twinning stress peak-to-peak (p-p) amplitudes of the mechanically cycled 10M $Ni_{50.0}Mn_{28.3}Ga_{21.7}$ [Publication VI].

In Publication V the magneto-mechanical uniaxial cycling of 10 M $Ni_{50.5}Mn_{28.0}Ga_{21.5}$ was performed in the specifically made test jig. The sample was extended against a pre-stressed spring at approximately 0.015 peak to peak (p-p) strain. The magnitude of the pre-stress was $\approx$ 1 MPa in this particular test. The strain decreased while cycling proceeded. This

was caused by the test system, as the shape-changing sample came in contact with the surfaces of the magnetic circuit, and the sample surface was damaged by wear. At certain cycle intervals, the sample was removed from the test jig for inspection. After restarting of the experiment the strain was recovered. The switching field H_{sw} value for the twin boundary motion in the sample increased due to cycling, although the results showed large deviation. The static MFIS at H_{appl}=1 T decreased from 0.053 to 0.043, which corresponds to a reduction in the deformed fraction of the sample by ≈ 20 %. In Publication VI it was shown that in mechanical cycling tests without surface wear MFIS remained at the original level of 0.06, when measured after $100 \cdot 10^6$ cycles. These results indicate the importance of mechanical wear of the sample surface in the long–term performance of the MSM element and the magnetic field induced twin boundary motion.

In another test which was conducted by using a magneto-mechanical test jig, the sample was cycled up to more than $200 \cdot 10^6$ cycles. The stroke was measured at specific intervals both at the cycling frequency *(dynamic)* and by manually adjusting the coil current *(static stroke)* [Publication V]. The twinning stress, which was calculated from the parameters obtained from the displacement - coil current loop, increased from 0.30 to 0.33 MPa during cycling. Instead of a gradual increase, the twinning stress increased abruptly at approximately $70 \cdot 10^6$ cycles.

3.2.3 Twinning induced cracking

Cracks were found to nucleate and grow on the specimen surface in both the magneto-mechanical and mechanical cycling [Publication V, Publication VI]. The evolution of the cracks in the magneto-mechanical cycling was studied by scanning electron microscope (SEM). The sample surface was studied before cycling and after a selected numbers of cycles. Round MnO inclusions (approximately 5 μm in diameter) were found in the specimens before cycling. As the twin boundaries were driven back and forth past the inclusions, microcracks initiated around the inclusions during the first millions of cycles, but these cracks did not usually not grow when the cycling continued.

Before the cycling, a few etch pits were present on the surface (Figure 3.13). They seemed to continue approximately as normal to the (001) surface (Figure 3.13*a*). The associated dislocation line is thus expected to be

the [001] direction. Also, etch marks resembling a cross were found, with the line grooves close to the [010] and [100] directions (Figure 3.13*b*).

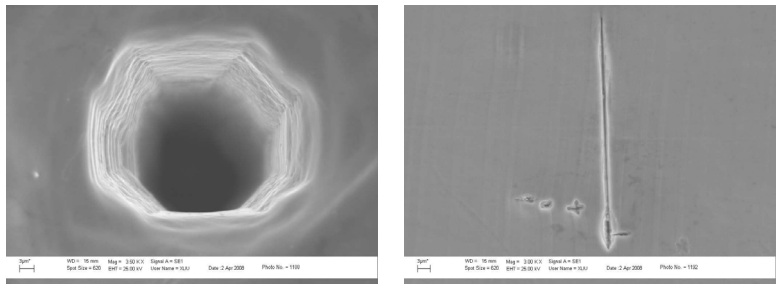

(a) (b)

Figure 3.13: SEM images of (a) a dislocation etch pit and (b) cross shaped etch marks on the $Ni_{50.5}Mn_{28.0}Ga_{21.5}$ (10M) sample surface in the material before magneto-mechanical testing. The surface is normal to (001) and the long axis of the stick sample is nearly horizontal in the images. Both pictures are secondary electron images (SEI).

All these etch pits are formed in the electropolishing of the sample. Therefore, the existence of the etch pits is evidence that some dislocations exist in the single crystals. The width of the pit in Figure 3.13*a* is about 35 μm, but 10 μm wide pits were also found. As the specimen has been prepared from a newly grown and heat treated single crystal ingot, dislocations are induced to the structure in the crystal growth process, during heat treatments or during the stick cutting and preparation.

The surface scratches were observed to strongly promote crack growth in cycling, in contrast to the inclusions, which were not found to effectively enhance crack growth. In Publication V the growth of the cracks on the surface occurred in the trace direction [011] of the twinning plane $K_1 = (011)$. Thus, the probable crack growth plane would be the twinning plane. This was confirmed by comparison of the XRD measurements and the SEM images of the cracks. The SEM study of the mechanical cycled samples in Publication VI showed on a detailed scale a step-wise growth of cracks along the twinning planes {101}, leading to gradual macroscopic crack growth in a direction close to 45° in respect to the loading axis [100]. In Publications V and VI, microcracks were observed in the surface scratches (Figure 3.14), some of them being present already before the cycling. Figure 3.14 shows that during cycling the microcracks have appeared at certain distances ($\approx 50\mu$m) along the scratch.

As a result of the crack growth the cross-sectional area carrying the load

Figure 3.14: Microcracks (indicated by arrows) at a surface scratch of 10M $Ni_{50.5}Mn_{28.0}Ga_{21.5}$ after magneto-mechanical cycling of 107 $\cdot 10^6$ cycles at $\epsilon_a \approx 1$ %. A secondary electron image (SEI).

decreases, and the local tensile stress at the crack tip increases. This enhances further the growth of the cracks and nucleation of the new cracks. This was confirmed in Publication VI, where several closely located cracks were found in the same region of the cycled samples. These multiple cracks led sometimes to the final fracture of the sample. In addition, crossing twin boundary configurations were observed in some mechanically cycled and cracked samples in Publication VI. This had led to formation of a macroscopic triangular shaped twin variant, which has its *c*-axis oriented sideways. This is the orientation of the *b*-axis of the usually existing twin variants, i.e. the variants with mutually compatible twin boundaries for the uniaxial cycling.

In Publication VI it was found that the MFIS does not decrease in a mechanically cycled sample, even if the cracks evolved in the sample. The macroscopic twin variant boundary in the cracked area was often terminated to the crack, if the twin boundary and the crack did not have the same direction. Examples of such twins terminating at the cracks are in Figure 3.15 which shows a micrograph of a 10M sample surface after $160 \cdot 10^6$ mechanical cycles.

In addition to the terminating twins, there is another new feature in the cycled twin structure. The original twin boundaries are between [100] and [001] twin variants, but new twins with perpendicular orientation have appeared at the right side crack of Figure 3.15. The pattern and direction of the twin and boundaries indicate that this new variant has [010] orientation, as described schematically in Figure 3.15*a*. In Figure 3.16*c*

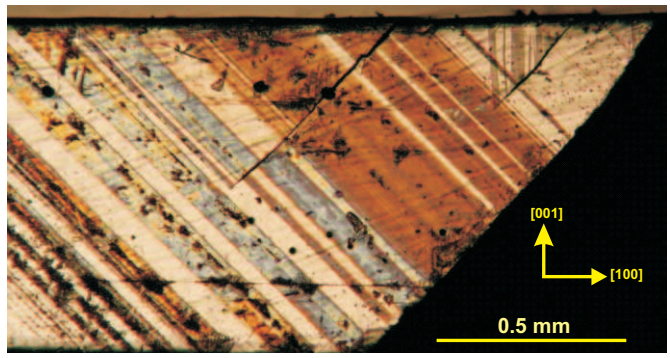

Figure 3.15: Twins terminating at cracks in a 10M material after cycling.

there is a SEM image of a mechanically cycled ($5.4 \cdot 10^6$ cycles) and cracked 10M sample $Ni_{50.0}Mn_{28.3}Ga_{21.7}$, showing the [100]-[010] twin boundaries on the fracture surface, which can be distinguished by their inclined orientations in the sample cross section. In Figure *b* there is a detailed SEM image of the same specimen as in Figure 3.16*c*, where the step-like morphology is visible. The step edges here seem to be close to [100] direction. In Figure 3.16*d* there is a SEM image of another 10M alloy crack surface ($160 \cdot 10^6$ cycles) [120], where the step-like morphology is also shown, but the step edges in this surface have at least an orientation partly close to <$01\bar{1}$>. The microscopic steps correspond to the {101} twinning planes and the height of the steps is along <101> direction, as described in the scheme of Figure 3.16*e*. A step-like morphology of the fatigue crack surfaces was found in all cracked fatigue specimens of Publications V, VI and [120], but the step edge directions can vary from one material to another. Finally, the remaining part of the cross section cracks in a brittle manner as shown in the lower part of Figure 3.16*d*.

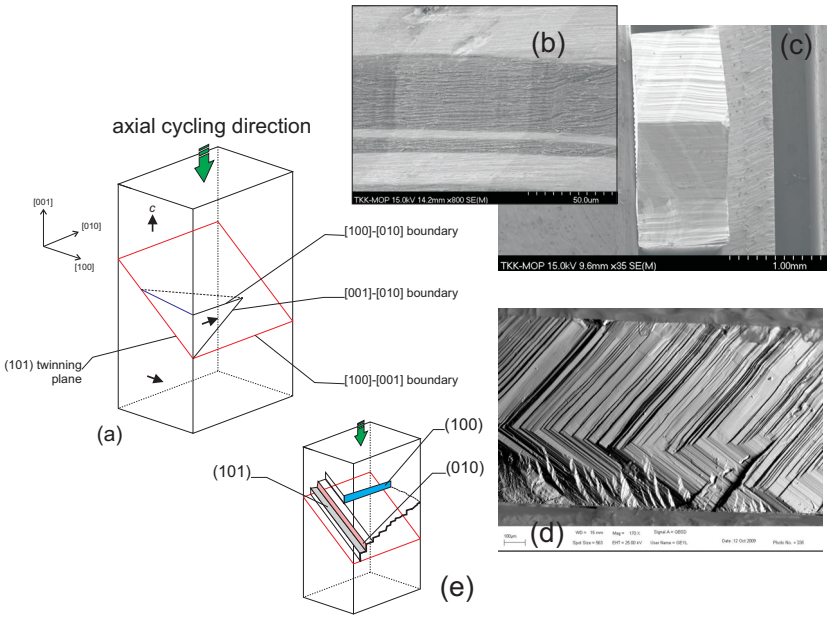

Figure 3.16: (a) Scheme of the twin variant areas and the twin boundary directions in a cycled sample. (b) A detailed SEM image of the broken 10M $Ni_{50.0}Mn_{28.3}Ga_{21.7}$ fatigue specimen with an overview SEM image of cracked surface (c). (d) A detail of another fatigue specimen with a step-like crack surface morphology. (e) A schematic presentation of the microscopic crack step planes of the crack surface.

4 Discussion

In Publication II, the switching field H_{sw} for magnetic-field-induced twin boundary motion in $Ni_{50.1}Mn_{27.7}Ga_{22.2}$ was found to be higher for the essentially single-variant state than for the two-variant state (Figure 3.1). This same effect was found both in the magnetic and mechanical measurements. The results in Figure 3.5 show that the magnitude of the calculated magnetic-field-induced stress and the mechanical stress are quite similar. According to Figure 3.1*a* the twinning stress of the essentially single-variant state sample at the onset of deformation is nucleation controlled, whereas the twinning stress is constant after the first twin boundary has nucleated. The obtained twinning strain in the essentially single variant state $\epsilon \approx 0.056$ % is similar to several published values, e.g. [121, 122]. The fact that in the two-variant state the pre-existing secondary twin variant decreases the calculated energy needed for the twin boundary motion, i.e. the onset value, supports this assumption.

In addition to these uniaxial compression results, the shear straining results presented in this Thesis (Figure 3.8) show a distinctively similar dependency on the variant state also in the shear mode. In Figure 3.8*a* the initiation peak exists in an essentially single variant untrained state, whereas in the trained state (Figure 3.8*b*) at the beginning of the shear there can be expected to exist narrow twins or twin boundary nuclei (e.g. at sites of existing material defects), in which state the twin boundary mobility is increased. It has been suggested [121] that it is not possible to obtain a fully single-variant state in 10M, and that there always exists a small amount of secondary twin variant. Due to hierarchical twinning, internal twin boundaries are expected to exist even in the nominally single-variant state [73], but their appearance, boundary orientation and width is different from the inter-variant twin boundaries which are visible in the optical microscope. Furthermore, since in these shear tests the specimen surfaces are fixed to the jig by glue, even a slight unparallelity of the jig surfaces could result in remnant twins in the fully sheared state

of a trained sample, but in the untrained state there should not exist such remnant twins, especially if the crystal is homogeneous, like in this case. Consequently, the shear stress peak of Figure 3.8*a* is considered to be caused by twin nucleation.

When the 10M martensite stick is in a two-variant state, i.e., with established twin variant boundaries, the mobility of the twin boundaries as measured by the triggering stress is material dependent. When the stick specimens are observed optically (or by a video camera), e.g., under uniaxial compression, the twinning behavior under monotonic straining is different in Ni-Mn-Ga alloys having a low twinning stress from those with a high twinning stress. In the constant strain rate compression experiments on the low twinning stress $Ni_{50.1}Mn_{27.7}Ga_{22.2}$ 10M single crystal specimens (the batch used in Publications II and V), the variant rearrangement was associated with only one or at most a few steadily moving twin boundaries. Also, the number of individual variant boundaries (and variant regions) remained small during the entire plateau. This plateau was flat for these specimens, while in the specimens with higher twinning stress the stress-strain curve increased more steeply. In the case of the specimens with this increasing twinning stress, new twin boundaries formed within the pre-existing variant, leading to a large number of thin separately nucleated twins. The location of the moving (i.e., active) boundary was also rapidly changing during straining. In summary, the stress in the detwinning plateau area of the $Ni_{50.1}Mn_{27.7}Ga_{22.2}$ single crystal sample having only one or two twin boundaries (e.g., Figure 3.1) is almost constant, when compared to the increasing twinning stress of an alloy having a large number of twin boundaries (see, e.g., Figure 5b of Publication III). However, there are exceptions and as an example of an uncommon behavior for the Ni-Mn-Ga samples, the nearly flat plateau of Figure 3.1 suggests that only the few existing boundaries move, and no nucleation of new variants occurs throughout the entire plateau [41]. In several sticks made of the same single crystal there were multiple twin boundaries present and the plateau was serrated with a gradually increasing twinning stress. If the grinding of the sample was made in too rough of a way, or the electropolishing was done to an insufficient level, the twinning stress remained high. Therefore, it is probable that in order to exhibit a constant twinning stress, the crystal quality has to be high and the surface stresses of the specimen have to be low.

In the repeated monotonic loadings shown in Figure 3.3 it was noticed

that the motion of the twin boundary may continuously need a high stress, when the boundary moves all the way through the sample. This suggests that instead of the high amount of energy necessary for the nucleation of the secondary variant, as is reported in Publication II, in a specific high quality single crystal 10M specimen $Ni_{50.4}Mn_{28.3}Ga_{21.3}$, the twinning stress may also be high during the continuous motion of twin boundary. The twinning stress may be at first very low when the fraction of the secondary twin variant is at the intermediate level. However, the twinning stress increases abruptly when the amount of the secondary variant is large (Figure 3.3). These results suggest that there may be different kinds of twin variant boundaries or mutually moving combined twin boundaries (e.g., which consist of more than a single twin boundary) in a high purity 10M material, which are moved at distinctively different stress levels. These low mobility boundaries are unstable in a high quality single crystal structure, since they appear and disappear during the training of the crystals. In lower quality 10M $Ni_{50.1}Mn_{29.0}Ga_{20.9}$ crystals, with obviously lower purity, the twinning stress did not once decrease to such extremely low values. As a consequence, the twin boundary mobility seemed to be more stable, although the explanation for this difference is not entirely clear. Similar results on 10M structure with a relatively stable twinning plateau but with a higher twinning stress have been previously reported in e.g. [52, 123, 124, 125]. So far, the instability of twinning stress has been reported only in the high quality crystals in [57].

When an increase in twinning stress observed in an essentially single-variant state [Publication II], or in the two-variant state single crystal (Figure 3.3), it suggests that the local microcracks or inhomogeneous twin variant structure may be generated in the material during straining. In the case of dynamic or cyclic straining, an abrupt change from the multivariant to the essentially single-variant state is possible if the strain regime of the Ni-Mn-Ga specimen is shifted by e.g. the influence of thermal expansion or contraction, by the changed external mechanical friction [Publication V] or by the increased internal dynamic stiffness at high number of cycles [Publication VI]. In Publication II it is suggested that especially the fatigue life of the MSM material at large strain amplitudes may be reduced, when the appearance of the single-variant state is likely. This can also be noticed in previously published cycling investigations [70].

The results of the shear stress tests (Figures 3.6 and 3.7) show that the

onset shear stress for twinning τ_{start}, the end shear stress value of the plateau τ_{finish}, and the twinning plateau width γ, all depend on the deformation history of the sample. They may even vary between different specimens made from the same crystal, although the heat treatment and procedures of preparing the sample were similar. These shear stress experiments were conducted with single crystal specimens cut essentially in the $< \bar{1}01 >$ direction ($K_1 = (101)$), which is the crystallographic direction of shear. This implies that the twin mobility in the material at a fixed temperature is not constant, but it depends on the deformation history, in addition to the other possible contributing factors such as defect distribution, twin configuration, or surface stress state. The mean twinning shear stress τ_t in the 10M $Ni_{49.9}Mn_{28.2}Ga_{21.9}$ samples varied from 0.55 to 0.94 MPa, with a reasonable 3.8 % shear strain error. The similar values for $Ni_{49.5}Mn_{29.4}Ga_{21.1}$ were τ_t = 0.23 to 0.58 MPa, excluding the untrained state single variant peak at 1.5 MPa. The twin configurations in Figures 3.10*b* and *c* show that twins with different twinning planes may appear. The different orientations of twins contributes to the differences in shear stress values required to move them.

In the present measurements direct shear has been applied, but the resolved shear stress could also be approximated by using Schmidt law [54]. The measured τ_t is about 60 % smaller than that given in the literature, while the measured γ is 2 to 3 times larger [54]. In several earlier publications, such as [55, 61, 126], higher twinning tensile or approximated shear stress values are reported for the 10M Ni-Mn-Ga structure than the present values of τ_t (e.g. in Figure 3.8) and σ_{tw} (e.g. in Figure 3.3). The experimentally measured maximum shear strain γ = 0.12 is about 7 % smaller than the value calculated with the lattice parameters (γ_0 = 0.13). The 7 % difference is not very large, and similar to previously reported uniaxial mode results, e.g. [121]. The difference of shear strain may be partly due to the fact that the specimen was glued from both sides to the shear test jig, and the hardened glue may have limited the deformation of the specimen near the surfaces. The recent efforts of the 10M single crystal Ni-Mn-Ga manufacturers to improve the crystal quality and production process has considerably reduced the twinning stress [57, 80]. It is thus reasonable to assume that the present low twinning stress values are a result of the improved crystal quality, higher homogeneity and purity.

Vibration damping ($\tan\delta$) in martensite and parent phase was studied

as a function of temperature for the Ni-Mn-Ga single crystal samples having 10M, NM or mixed martensite structure in Publication III. In all these materials $\tan\delta$, E' and E'' are temperature dependent. The twin boundary mobility of 10M martensite increases with temperature both in monotonic and dynamic loading, when heated towards the parent phase area, as the lattice tetragonality decreases and the interatomic distances of the moving atoms in the vicinity of the twin boundary decrease [100]. In the studied NM martensite specimens, the high damping region extended to a higher temperature (approximately 385 K or 410K, depending on the alloy) than in the studied 10M material (approximately 315 K). When the martensites are heated, there is a drop in the dynamic modulus E' near the phase transformation region, which is related to phonon softening. Damping in the parent phase is generally low, as the mobile twin boundaries do not exist. When the specimen is dynamically loaded and cooled from the parent phase in the DMA system, $\tan\delta$ in the NM specimens is slightly larger than when measured prior to heating to the parent phase. In the 10M and mixed specimens, the $\tan\delta$ level is retained after phase transformation from parent to martensite phase. We suggest this difference to be related to the higher twinning stress and higher E' of the NM martensite when compared to the 10M martensite. The specimens were cycled with limited applied force amplitude, and thus, the accommodation of the martensite variants is expected to happen at a lower stress in the 10M than in the NM martensite, due to the lower twinning stress of the 10M martensite [54].

The accommodation of twin variants with the applied cyclic stress is expected to enhance the motion of twin boundaries, similar to training in the monotonic case in e.g. [127]. In the NM specimens, the accommodation of twin variants can essentially occur only after the dynamic modulus E' decreases to a low enough level, and the accommodation is probably further enhanced when the martensite transformation occurs under dynamic loading. This proposed behavior resembles the thermo-mechanical training by monotonic loading. Thus, damping of the NM martensite could be higher after the MT than before the transformation, as the results in Publication III show. In the specimens with the 10M and mixed martensite structure, however, the accommodated state is reached already before the transformation to the parent phase.

According to Publication IV, the $\tan\delta$ values of martensite in dynamic loading increase at a greater rate with increasing amplitude when tem-

perature raises. This is a consequence of the decreasing twinning stress, i.e., the onset for martensite twin boundary motion decreases with increasing temperature [Publication III][59]. However, the strain-amplitude dependency at different temperatures is essentially similar (Figure 3.11). Based on the linear relation of the secondary variant fraction and the strain in the uniaxial loading of the 10M Ni-Mn-Ga single crystal sample [52], the total traveled distance of the twin boundary, or the sum of the distances traveled by many boundaries, is directly dependent on strain. In bending, a linear relationship also exists between the bending strain (by the variant accommodation) and the variant fraction. With the sinusoidal straining at a constant frequency, the distance traveled by the twin boundaries increases linearly with growing amplitude. The similar trend of the martensite damping at different temperatures suggests that the damping properties in these martensitic Ni-Mn-Ga alloys essentially depend on the extent of the twin boundary motion. As the $\tan\delta$ of the cubic parent phase is two orders lower than that of the martensitic phase, it can be suggested that the main contributor to the high damping in the martensite phase is correlated to its structure, and especially to the hysteretic motion of twin boundaries. This is further supported by the fact that there seems to be a threshold level for the high damping, in the example (Figure 3.11), approximately at ϵ_a = 0.02. When the ϵ_a increases to the level 0.10–0.25, the rate of increase of damping slows down. It is assumed that here the ϵ_0 level of NM structure is reached, beyond which the twin-boundary-based straining cannot occur.

Magneto-mechanical cycling, based on the extending of the specimen by the magnetic shape memory effect and contraction by a spring force, can also be applied to 10M Ni-Mn-Ga alloys [Publication I, Publication V]. The long-term behavior of these alloys has been well evaluated also in the mechanical cycling [Publication VI]. The fatigue life of the 10M single crystals with mobile twin boundaries is long compared to many other metal alloys. Cyclic mechanical straining of 2 % peak-to-peak strain was applied for $2{\cdot}10^9$ cycles without breaking of the sample, although microcracking and clear changes in the twin structure occurred. Magnetic field-induced strain remains in the original level in a cycled sample when surface wear during cycling is eliminated. However, with the ultra-low twinning stress 10M material the fatigue life of individual specimens showed a large variation [Publication VI]. Fatigue tests with very homogeneous crystals $Ni_{50.4}Mn_{28.0}Ga_{21.6}$ showed even more variation of fatigue

life [120]. With these results it has been confirmed that the differences in the material structure have an influence on the twin boundary motion in cycling, as was earlier presented as a hypothesis.

It was found in Publication V that grinding of the MSM specimen surface reduced the obtainable magnetic field induced strain (MFIS) in cycling. Grinding creates surface and subsurface damage associated with a stress field on the surface. As a hypothesis it is presented that this hinders motion of the partial dislocations needed for the twin boundary propagation [128], and thus, reduces the mobility of twin boundaries. The observed decrease of the MFIS with cycling induced damage supports this assumption, as well as the fact that also the area of the worn surface seems to correlate with the decrease of MFIS. The crystal lattice in the scratch area is perturbed by the stress field of the associated dislocations [129]. With this assumption, the stress constraint and the perturbation at the scratch would be partly released by the microcracks forming at the scratch. The distance between these microcracks would be thus associated with the magnitude of this stress field. The observation of the evenly distributed microcracks at the scratch of the fatigue sample in Figure 3.14 supports this assumption. Furthermore, since the motion of twin boundary can be associated with shuffling and de-shuffling motion of the atoms [32] the perturbed crystal lattice at the scratch could hinder the motion of a twin boundary moving through this region.

In Publication VI, the changes of twinning stress in mechanical cycling occurred mostly in coincidence with abrupt changes in the dynamic stress and strain of the sample. A decrease of the twinning stress was associated with the decrease of applied external stress and strain, and vice versa (Figure 3.12). This result confirms the interdependency of twinning stress and strain, which was also found in the vibration damping measurements [Publication IV]. One explanation for this is the different local twin boundary motion resistance in the material due to the structural inhomogeneity. The structural variation and high inhomogeneity has been observed by neutron diffraction measurements even in a high quality Ni-Mn-Ga crystal [130]. Such changes in the structure promote the inhomogeneous nucleation of twins. When these differences take place in the different regions of the MSM sample, there will be locations with easy and hard moving twins. If the resistance to twin boundary motion, i.e, the twinning stress, in a certain region remains constant, and the twin boundaries are mobile only in a specific region of the sample, it could

be presumed that the defects hindering the twin boundary motion are at fixed positions in the solid state lattice and that their amount does not change. However, as shown in Publication II, when the strain is decreased or increased, the regions of easily moving twin boundaries must change their location due to the interdependency of the variant fractions and the strain. Since the resistance of the movement in the new region may differ from that of the original one, also a change of the twinning stress, applied stress and strain takes place.

In Publication VI a gradual stiffening of the sample was observed in cycling up to several tens of 10^6 cycles. This was shown to be associated with the decrease of the twin variant width in the sample, i.e., refining of the twins. The refining may occur in different regions of the sample, having varying resistances to the twin boundary motion. When an external stress is applied to the sample, at first the twin boundary with the lowest resistance (i.e. twinning stress) starts to move. If the twin boundary then moves to a region with a higher resistance for its motion, more stress is needed for further movement - or if it moves to the region with lower mobility, the stress needed decreases. Alternatively, there may be another twin boundary, which starts to move as the energy needed for its motion is exceeded, or a new twin boundary may then nucleate if that is energetically preferable. Nucleation is expected to occur especially at intersections of slip lines or near lattice defects, where the local stress may be higher than in the heterogeneous twinning [41]. Thus, in the cyclic long-term straining of Ni-Mn-Ga material, the twin boundary motion is associated with a gradually increasing stress with the refining of twin structure, as new and thinner twins are nucleated. This evolution is associated with the accumulation of local defects in the sample, i.e. the movement of boundaries creates defects in the active regions causing movement to spread to other region with higher twinning stress.

Crack growth in the Ni-Mn-Ga 10M martensite single crystals occurred along steps usually associated with the twinning planes [Publication VI], which was also observed in the magneto-mechanical and mechanical cycling. The fatigue crack growth in the 10M single crystal Ni-Mn-Ga can occur in several ways, and were found to depend on the orientation of twin boundaries, the scratches of the specimen surface, inclusions and other irregularities of the structure. This supports the presented hypothesis that twinning fatigue results in microstructural changes that influence the twin mobility and the long-term performance of the material.

In Publication VI the microstructural cracks, which evolved during cycling, did not have a significant effect on the MFIS. The continuous twin boundary may end at the crack surface, instead of continuing across the entire sample. The crack surface acts for the twin as a free surface where there is no coherency requirement for reducing the twin boundary surface energy. However, the twin boundaries on both sides of the crack may still be mobile, allowing the MFIS. Actually, as cracking may release the lattice constraints caused by the large defects, it can even enhance twin mobility. The SEM examination of some samples in the magneto-mechanical cycling Publication V revealed some MnO type inclusions of the specimen surface. Some of them were removed probably in the sample preparation, and in magneto-mechanical cycling the surface microcracks were observed to have grown from such cavities or inclusions, as shown in Figure 4.1.

Figure 4.1: Microcracks at a surface cavity of the $Ni_{50.5}Mn_{28.0}Ga_{21.5}$ specimen after $10.5 \cdot 10^6$ magneto-mechanical cycles with 1 % p-p strain (a bright field secondary electron image).

A hard inclusion inside the twinned martensitic material is not expected to deform alike its surroundings, and an increased local lattice constraint can nucleate a crack near the inclusion. If such microcracks are located along the path of a growing crack, the crack could partly grow by the successive adjoining of the microcracks, which would lead to an uneven crack surface. Growth of macroscopic cracks at the sites of crystal defects may be explained by a similar principle, although the actual verification is not easy, as it is not the only mechanism for the crack growth. Another growth method may be related to the increased stress concentration due

to the lattice misfit of the intersection of the compatible and the incompatible (i.e., blocking) twin variants. Nucleation of microcracks by twinning has been reported in other materials [41].

Based on the macroscopic twinning on K_1 planes, when the load is applied along the 001 direction of 10M martensite the twin is equally likely to nucleate on any of the four twinning planes that are non-parallel with the applied stress. Considering this, a blocking twin [41], i.e., a third variant may nucleate on a crossing twinning plane and it can extend freely through the stick as long as it does not collide with an existing twin boundary. The blocking twin will block the twin boundaries from moving through it. Thus, the twinning strain decreases by an amount determined by the size of the blocking twin.

Furthermore, it is noteworthy that the rotational component due to twinning in the single crystal may contribute to the appearance of the third variant type if the crystal is constrained. In the 10M martensite structure the twin boundary involves a surface tilt of approximately 3.5 or 7 $^\circ$ (depending on the variants and lattice parameters). For example, supposing that in an originally single variant state rectangular stick cut in the <001> direction there is a single twin boundary between the [100] and [001] variants, and the end surfaces of the stick have the corresponding tilt angle between each other (Figure 4.2). If the stick is compressed between parallel surfaces, such as in a magneto-mechanical prestress-type actuator, the stress on the tilted surfaces will not be evenly distributed. Therefore, the stress concentration can be partly accommodated by the nucleation of a new [010] twin variant, which can in the framework of the moving twin boundaries be of an incompatible orientation with the existing ones, i.e. it is a blocking third variant. The stress concentration described above increases with the stick width, mainly with the width in the *a*-*c*-plane, and with thin specimens the effect is not expected to be large.

In summary the crossing twin boundaries are usually expected to lead to the interlocked state, i.e. increase of the stress is needed to move the twin boundaries when strained, and to promote cracking. However, as there are several factors influencing the formation of the crossing twin boundaries, no single reason for their appearance can be given.

Yet there is still another reason for the cracks to nucleate and grow provided by the theory of the pile-up of twinning dislocations or disconnections, which have been proposed to allow the motion of twin bound-

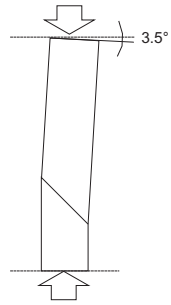

Figure 4.2: Surface tilting by a twin boundary (schematic).

aries [53]. With a sufficient back-stress, the growing pile-up could eventually nucleate a crack on the plane containing the disconnection wall. Of course, it is possible that several of the proposed reasons are mutually interacting. In a material with some impurities such as oxygen, the twinning dislocation pile-ups could be generated at the MnO inclusions. Furthermore, there are the observed etch pits on the sample surface before cycling. In Figure 3.13 the orientation of the etch pit cavity, extending into the inside of the <100> oriented sample, appears to be [100]. According to the literature [46], the square shape of the etch pit is characteristic for $\{100\}_M$ plane on which it forms in a material with a cubic lattice. The etch pit in Figure 3.13*a* has an octagonal shape. Due to the lattice misfit and elastic energy of the dislocation, the dislocation line is chemically a more active region than a stress free region. Thus, the line of the dislocation in Figure 3.13a may be assumed to be in the [100] direction. Together with the influence of the incompatible variant presented before, these sessile [100] dislocations could perhaps lead to the twinning dislocation pile-up, and thus allowing cracking in very high purity samples where no inclusions exist. When cycled further, a new pile-up could appear at the end of the existing crack. The pile-up would be released when the crack grows further a suitable distance, and repetition of this event results in a step-like crack growth. As was observed in this Thesis, the crack grows along twinning planes, and thus suggests that the new pile ups would appear on the suitable twinning plane, which in each stage of the crack propagation is most convenient. A proposed mechanism for generation of the pile-up by the moving twin boundary and the sessile [100] dislocation is illustrated in Figure 4.3. Such kind of cracking has been recently reported in [120], but the actual mechanism of the cracking is not yet clear.

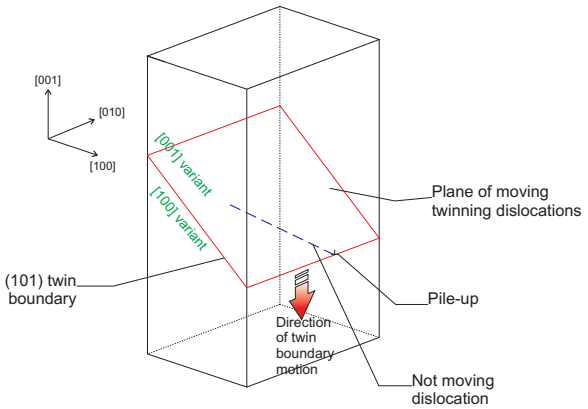

Figure 4.3: A schematic illustration of the moving twin boundary and the proposed generation of the twinning dislocation pile-up in a 10M Ni-Mn-Ga single crystal. The material contracts vertically as the twin boundary moves in the direction of the arrow.

5 Conclusions

Based on the results presented in this Thesis and attached publications the following conclusions may be drawn:

- The onset stress of twin boundary motion of Ni-Mn-Ga 10M martensitic single crystal is higher and controlled by the twin nucleation in the single variant state, when compared to the case where there are previously nucleated twin boundaries. This feature is more pronounced in a low twinning stress crystal. Extensive training (i.e., back and forth straining) reduces the high onset stress, probably because twin nuclei are created in the crystal, and the start of the twin boundary motion thereafter is not any more controlled by twin nucleation. Furthermore, in a low twinning stress crystal, the (nucleated) twin boundary can move at almost a constant stress. The twinning stress may be in this case very low but the variation of the twinning stress and the instability of twin boundaries increases. It was suggested that the decreased mobility of an unstable twin boundary is related to an additional twin variant being introduced to the boundary. In a high twinning stress crystal the deformation occurs as a consequence of the motion of multiple twin boundaries having different onset stresses. Boundaries move under changing strain one after another, at increasing stress. A similar trend of an increasing stress with strain and simultaneous thinning of twins was found in the long-term fatigue specimens, showing that during fatigue the accumulating defects cause a corresponding change in the twinning stress of the crystal.

- Twinning of Ni-Mn-Ga 10M martensite was experimentally studied for the first time under simple shear. The onset stress for twin boundary motion was observed to have large variation in the low twinning stress alloy, depending on the twin variant configuration. The stress onset for twinning in these alloys could in the trained

state be very low (τ = 0.07 to 0.23 MPa). In the higher twinning stress 10M Ni-Mn-Ga alloy the variation of the stress onset was smaller, and the stress onset for twinning was higher (τ > 0.60). It can be concluded that a similar effect of the nucleation stress to onset stress for twin boundary motion exists in deformation both under the shear mode and under the uniaxial mode. The measured maximum twinning shear strain γ was 0.12 and the corresponding value at uniaxial strain ϵ was approximately 0.06.

- It was discovered that the twin mobility is lower and the twins also nucleate during straining in 10M martensite Ni-Mn-Ga crystals, which show less perfect crystal modulation than the homogeneous crystals. In these crystals the macroscopic twins are proposed to be nucleated by the inhomogeneous mechanism, whereas the homogeneous nucleation cannot be excluded in the high quality crystals.

- Damping ($\tan\delta$) of the Ni-Mn-Ga martensite is essentially based on the hysteretic twin boundary motion and thus the loss tangent increases with vibration strain amplitude up to the crystallographic limit ϵ_0. The mobility of twins in 10M martensite Ni-Mn-Ga is higher than in the non-modulated martensite. The high damping regime is found above the twinning stress, typically in 10M at lower stresses σ of $\approx$ 1 MPa, when compared to the non-modulated martensite with the stress level of 20 MPa. Tan δ of martensite can be high and depends on temperature, since the mobility of martensite twin boundaries increases with increasing temperature. In the parent phase this increase of damping with the amplitude does not exist. There is a threshold strain level for the increased damping of typically $\Delta\epsilon \approx 0.02$. Both magneto-mechanical and mechanical uniaxial cycling of 10M Ni-Mn-Ga eventually causes fatigue crack growth which microscopically occurs along steps close to the {101} twinning planes. Surface microcracks are nucleated by inclusions or scratches. The fatigue cracks typically grow in a $\approx 45\,^{\circ}$ direction in relation to the loading axis.

- Ni-Mn-Ga material has potentially a long fatigue life. The so far highest reported number of cycles ($2 \cdot 10^9$) with a single crystal Ni-Mn-Ga fatigue specimen was recorded. However, if the cycling conditions are not carefully considered, the fatigue life can be significantly shortened. Several reasons for the shortening of the fatigue

life were confirmed or proposed, such as the specimen damage by surface wear, adjoining of fatigue cracks, cracking by the influence of incompatible twin variant and increased internal stress during the twin nucleation in the essentially single variant state.

The results of the present Thesis contribute to the scientific understanding and shed light on the possibilities for utilizing and further improvements to Ni-Mn-Ga magnetic shape memory materials both in monotonic and dynamic use. Based on the presented results, it can be concluded that in order to ensure the repeatability and consistent magneto-mechanical properties, the creation of large enough twin nuclei by e.g. a training treatment of 10M Ni-Mn-Ga crystals is necessary especially in high quality crystals, so that the twinning onset stress is reduced to a stable level. In addition, for ensuring the performance of material in continuous use, and for avoiding the increased internal stress connected to the single variant state or the abruptly appearing hard moving twin boundary, the application of Ni-Mn-Ga material and the possibility of wear of the specimen surfaces should be taken into account already in the design phase of the potential actuator or respective apparatus. The high sensitivity of the twin boundary motion to the crystal structure, defects and impurities, tends to cause variation in the magneto-mechanical properties especially when the material has very low twinning stress, and consequently this issue is a challenge for the industrial utilization of Ni-Mn-Ga MSM materials. For vibration damping applications, especially in the case of non-modulated Ni-Mn-Ga martensite, the allowed twinning stress levels are higher and the properties of the specimens are easier to control.

Bibliography

[1] G. B. Olson and W. S. Owen. *Martensite*. ASM International, Materials Park, Ohio, 1992.

[2] K. Bhattacharya. *Microstructure of martensite*. Oxford University Press, 2003.

[3] K. Otsuka and C. M. Wayman. *Shape Memory Materials*. Cambridge University Press, Cambridge, UK, 1998.

[4] V. V. Kokorin, V. V. Martynov, and V. A. Chernenko. Stress-induced martensitic transformations in nickel manganese gallium (Ni_2MnGa). *Scripta Metallurgica et Materialia*, 26(2):175–177, 1992.

[5] V. A. Chernenko, J. Pons, E. Cesari, and K. Ishikawa. Stress-temperature phase diagram of a ferromagnetic Ni-Mn-Ga shape memory alloy. *Acta Materialia*, 53(19):5071–5077, 2005.

[6] K. Inoue, K. Enami, Y. Yamaguchi, K. Ohoyama, Y. Morii, Y. Matsuoka, and K. Inoue. Magnetic-field-induced martensitic transformation in Ni_2MnGa-based alloys. *Journal of the Physical Society of Japan*, 69(11):3485–3488, 2000.

[7] M. Matsumoto, J. Tani, T. Takagi, and K. Yamauchi. NiMnGa alloy with a controlled finish point of the reverse transformation and shape memory effect, Sep 23 1998 1998. Patent appl. EP0866142A1.

[8] R. Kainuma, Y. Imano, W. Ito, Y. Sutou, H. Morito, S. Okamoto, O. Kitakami, K. Oikawa, A. Fujita, T. Kanomata, and K. Ishida. Magnetic-field-induced shape recovery by reverse phase transformation. *Nature*, 439(7097):957–960, 2006.

[9] V. V. Kokorin, V. A. Chernenko, E. Cesari, J. Pons, and C. Segui. Premartensitic state in Ni-Mn-Ga alloys. *Journal of Physics: Condensed Matter*, 8(35):6457–6463, 1996.

[10] V. V. Kokorin. Structural phase transformations in Ni-Mn-Ga alloys. *Solid-Solid Phase Transformations, International Conference on Solid-Solid Phase Transformation, 4th, Kyoto, Japan, May 24-28, 1999*, pages 1100–1107, 1999.

[11] Fr. Heusler. Über den Zusammenhang der magnetischen und mechanischen Eigenschaften der gewalzten Heusler-Bronze (Mangan-Aluminium-Kupfer). *Zeitschrift fur Physik A Hadrons und Nuclei*, 10(1):403–404, 1922.

[12] A. J. C. Wilson, editor. *Structure reports (Strukturbericht)*, volume 13. Oosthoek's uitgevers mij, Published for the International Union of Crystallography, 1954.

[13] P. J. Webster, K. R. A. Ziebeck, S. L. Town, and M. S. Peak. Magnetic order and phase-transformation in Ni_2MnGa. *Philosophical magazine B*, 49(3):295–310, 1984.

[14] F. A. Hames. Ferromagnetic-alloy phases near the compositions Ni_2MnIn, Ni_2MnGa,Co_2MnGa, Pd_2MnSb, and PdMnSb. *Journal of Applied Physics*, 31:370S–371S, 1960.

[15] P. J. Webster. Heusler alloys. *Contemporary Physics*, 10(6):559–577, 1969.

[16] J. Soltys. Effect of heat treatment on the atomic arrangement and the magnetic properties in nickel-manganese-gallium (Ni_2MnGa). *Acta Physica Polonica, A*, A47(4):521–523, 1975.

[17] R. W. Overholser, M. Wuttig, and D. A. Neumann. Chemical ordering in Ni-Mn-Ga Heusler alloys. *Scripta Materialia*, 40(10):1095–1102, 1999.

[18] B. Ingale, R. Gopalan, M. Rajasekhar, and S. Ram. Studies on ordering temperature and martensite stabilization in $Ni_{55}Mn_{20-x}Ga_{25+x}$ alloys. *Journal of Alloys and Compounds*, 475(1-2):276–280, 2009.

[19] I. Aaltio, O. Söderberg, M. Friman, I. Glavatskyy, Y. Ge, N. Glavatska, and S.-P. Hannula. Determining the liquidus and ordering temperatures of the ternary Ni-Mn-Ga and quaternary Ni-Mn-Ga-Fe/Cu alloys. In P. Sittner, editor, *Proc. ESOMAT 2009*, pages 04001–1–04001–6, 7-11 September 2009.

[20] G. Erdelyi, H. Mehrer, A. W. Imre, T. A. Lograsso, and D. L. Schlagel. Self-diffusion in Ni_2MnGa. *Intermetallics*, 15(8):1078–1083, 2007.

[21] M. L. Richard. *Systematic analysis of the crystal structure, chemical ordering, and microstructure of Ni-Mn-Ga ferromagnetic shape memory alloys*. PhD thesis, Massachusetts Institute of Technology, 2005.

[22] J. Chen, Y. Li, J.-X. Shang, and H.-B. Xu. Site preference and alloying effect of excess Ni in Ni-Mn-Ga shape memory alloys. *Chinese Physics Letters*, 26(4), 2009.

[23] J. Enkovaara. *Atomistic simulations of magnetic shape memory alloys*. PhD thesis, Helsinki University of Technology, Espoo, Finland, 2003.

[24] V. A. Chernenko. Compositional instability of beta-phase in Ni-Mn-Ga alloys. *Scripta Materialia*, 40(5):523–527, 1999.

[25] P. Entel, V.D. Buchelnikov, V.V. Khovailo, A.T. Zayak, W.A. Adeagbo, M.E. Gruner, H.C. Herper, and E.F. Wassermann. Modelling the phase diagram of magnetic shape memory Heusler alloys. *J. Phys. D: Appl. Phys*, 39:865–889, 2006.

[26] V. V. Kokorin, I. A. Osipenko, and T. V. Shirina. Phase transitions in alloys $Ni_2MnGa_xIn_{1-x}$. *Physics of Metals and Metallography (translation of Fizika Metallov i Metallovedenie)*, 67(3):173–176, 1989.

[27] C. Segui, J. Pons, and E. Cesari. Effect of atomic ordering on the phase transformations in Ni-Mn-Ga shape memory alloys. *Acta Materialia*, 55(5):1649–1655, 2007.

[28] J. Pons, V. A. Chernenko, R. Santamarta, and E. Cesari. Crystal structure of martensitic phases in Ni-Mn-Ga shape memory alloys. *Acta Materialia*, 48(12):3027–3038, 2000.

[29] A. Sozinov, A. A. Likhachev, and K. Ullakko. Crystal structures and magnetic anisotropy properties of Ni-Mn-Ga martensitic phases with giant magnetic-field-induced strain. *IEEE Transactions on Magnetics*, 38(5, Pt. 1):2814–2816, 2002.

[30] N. Lanska, O. Söderberg, A. Sozinov, Y. Ge, K. Ullakko, and V. K. Lindroos. Composition and temperature dependence of the crystal structure of Ni-Mn-Ga alloys. *Journal of Applied Physics*, 95(12):8074–8078, 2004.

[31] O. Söderberg, A. Sozinov, N. Lanska, Y. Ge, V. K. Lindroos, and S.-P. Hannula. Effect of intermartensitic reaction on the co-occurrence of the magnetic and structural transition in Ni-Mn-Ga alloys. *Materials Science and Engineering: A*, 438-440:957–960, 2006.

[32] M. Han, J. C. Bennett, M. A. Gharghouri, J. Chen, and C. V. Hyatt. Understanding modulated twin transition at the atomic level. *Acta Materialia*, 55(5):1731–1740, 3 2007.

[33] Y. Ge. *The crystal and magnetic microstructure of Ni-Mn-Ga alloys*. PhD thesis, Helsinki University of Technology, Espoo, 2007.

[34] L. Righi, F. Albertini, G. Calestani, L.Pareti, A. Paoluzi, C. Ritter, P. A. Algarabeland L. Morellon, and M. R. Ibarra. Incommensurate modulated structure of the ferromagnetic shape-memory Ni_2MnGa martensite. *Journal of Solid State Chemistry*, 179:3526–3534, 2006.

[35] S. Kaufmann, U.K. Rössler, O. Heczko, M. Wuttig, J. Buschbeck, L. Schultz, and S. Fähler. Adaptive modulations of martensites. *Physical Review Letters*, 104(14):145702, 2010.

[36] A.G. Khachaturyan, S.M. Shapiro, and S. Semenovskaya. Adaptive phase formation in martensitic transformation. *Phys.Rev.B*, 43:10832, 1991.

[37] A. Sozinov, A. A. Likhachev, and K. Ullakko. Magnetic and magnetomechanical properties of Ni-Mn-Ga alloys with easy axis and easy plane of magnetization. *Proceedings of SPIE-The International Society for Optical Engineering*, 4333(Active Materials: Behavior and Mechanics):189–196, 2001.

[38] V. V. Martynov and V. V. Kokorin. The crystal structure of thermally- and stress-induced martensites in nickel-manganese-gallium (Ni_2MnGa) single crystals. *Journal de Physique III*, 2(5):739–749, 1992.

[39] A. T. Zayak and P. Entel. Role of shuffles and atomic disorder in Ni-Mn-Ga. *Materials Science & Engineering, A*, A378(1-2):419–423, 2004.

[40] R. W. Cahn. Twinned crystals. *Advances in Physics, supplement of Philosophical Magazine*, 3(12):363–445, 1954.

[41] J. W. Christian and S. Mahajan. Deformation twinning. *Progress in Materials Science*, 39(1-2):1–157, 1995.

[42] S. Kibey, J. B. Liu, D. D. Johnson, and H. Sehitoglu. Predicting twinning stress in fcc metals: Linking twin-energy pathways to twin nucleation. *Acta Materialia*, 55(20):6843–6851, 2007.

[43] N. Okamoto, T. Fukuda, and T. Kakeshita. Magnetocrystalline anisotropy and twinning stress in Ni-Mn-Ga ferromagnetic shape memory alloys. *Journal of Physics: Conference Series*, 51:315–318, 2006.

[44] M. Bevis and A. G. Crocker. Twinning modes in lattices. *Proceedings of the Royal Society of London, Series A, Mathematical and physical sciences*, 313:509–529, 1969.

[45] G.R. Barsch and J.A. Krumhansl. *Martensite*, chapter Nonlinear physics in martensitic transformations, pages 125–147. ASM International, 1992. Ed:s: G.B. Olson AND W.S. Owen.

[46] G. Gottstein. *Physical foundations of materials science*. Springer-Verlag, Heidelberg, 2004.

[47] J. W. Christian. *Encyclopedia of materials: Science and technology*, chapter Twinning: Crystallography, pages 9423–9425. Elsevier Science Ltd., 2001.

[48] B. A. Bilby and A. G. Crocker. The theory of the crystallography of deformation twinning. *Proceedings of the Royal Society of London, Series A, Mathematical and physical sciences*, 288:240–255, 1965.

[49] P. Müllner and A.H. King. Deformation of hierarchically twinned martensite. *Acta Materialia*, 58:5242–5261, 2010.

[50] A. Kelly, G. W. Groves, and P. Kidd. *Crystallography and crystal defects*. John Wiley & Sons Ltd., Chichester, UK, 2000.

[51] D.Y. Cong, Y.D. Zhang, Y.D. Wang, C. Esling, X. Zhao, and L. Zuo. Determination of microstructure and twinning relationship between martensitic variants in 53 at.-% Ni 25 at.-% Mn 22 at.-% Ga ferromagnetic shape memory alloy. *Journal of Applied Crystallography*, 39(5):723–727, 2006.

[52] P. Molnar, P. Sittner, P. Lukas, S-P. Hannula, and O. Heczko. Stress-induced martensite variant reorientation in magnetic shape memory Ni-Mn-Ga single crystal studied by neutron diffraction. *Smart materials and structures*, 17(3):035014–1–5, 2008.

[53] P. Müllner. Between microscopic and mesoscopic descriptions of twin-twin interaction. *Z. Metallkd.*, 97(3):205–216, 2006.

[54] N. Okamoto, T. Fukuda, and T. Kakeshita. Temperature dependence of rearrangement of martensite variants by magnetic field in 10M, 14M and 2M martensites of Ni-Mn-Ga alloys. *Materials Science and Engineering: A*, 481-482:306–309, 2008.

[55] K. Koho, J. Vimpari, L. Straka, N. Lanska, O. Söderberg, O. Heczko, K. Ullakko, and V. K. Lindroos. Behaviour of Ni-Mn-Ga alloys under mechanical stress. *Journal de Physique IV: Proceedings*, 112(International Conference on Martensitic Transformations, 2002, Part 2):943–946, 2003.

[56] L. Dai. *Elasticity in ferromagnetic shape memory alloys*. PhD thesis, University of Maryland, 2004. http://hdl.handle.net/1903/2047.

[57] L. Straka, N. Lanska, K. Ullakko, and A. Sozinov. Twin microstructure dependent mechanical response in Ni-Mn-Ga single crystals. *Applied Physics Letters*, 96(13):131903, 2010.

[58] S. A. Wilson, R. P. J. Jourdain, Q. Zhang, R. A. Dorey, C. R. Bowen, M. Willander, Q. Ul Wahab, S. M. Al-hilli, O. Nur, E. Quandt, C. Johansson, E. Pagounis, M. Kohl, J. Matovic, B. Samel, W. van der Wijngaart, E. W. H. Jager, D. Carlsson, Z. Djinovic, M. Wegener, C. Moldovan, R. Iosub, E. Abad, M. Wendlandt, C. Rusu, and K. Persson. New materials for micro-scale sensors and actuators: An engineering review. *Materials Science and Engineering: R: Reports*, 56(1-6):1–129, 2007.

[59] I. Aaltio, J. Tellinen, K. Ullakko, and S.-P. Hannula. Deformation properties of magnetic shape memory materials used in actuators. In H. Borgmann, editor, *Proc. 10th Int. Conference on new actuators, ACTUATOR 2006*, pages 402–405, Bremen, Germany, 14-16 June 2006. HVG Hanseatische Veranstaltungs-GmbH.

[60] T. Kakeshita and T. Fukuda. Energy evaluation for twinning plane movement under magnetic field in ferromagnetic shape memory alloys. *International Journal of Applied Electromagnetics & Mechanics*, 23(1):45–50, 2006.

[61] L. Straka. *Magnetic and magneto-mechanical properties of Ni-Mn-Ga magnetic shape memory alloys*. PhD thesis, Helsinki University of Technology, Espoo, 2007. http://lib.tkk.fi/Diss/2007/isbn9789512288205.

[62] O. Heczko, L. Straka, O. Söderberg, and S.-P. Hannula. Magnetic shape memory fatigue. In *Smart Structures and Materials 2005 - Active Materials: Behavior and Mechanics, Mar 7-10 2005*, volume 5761, pages 513–520, San Diego, CA, United States, 2005. International Society for Optical Engineering.

[63] O. Söderberg, Y. Ge, A. Sozinov, S.-P. Hannula, and V. K. Lindroos. Recent breakthrough development of the magnetic shape memory effect in Ni-Mn-Ga alloys. *Smart Materials and Structures*, 14(5):223–235, 2005.

[64] N. Glavatska, G. Mogylny, I. Glavatskiy, and V. Gavriljuk. Temperature stability of martensite and magnetic field induced strain in Ni-Mn-Ga. *Scripta Materialia*, 46(8):605–610, 2002.

[65] M. A. Meyers, O. Vöhringer, and V. A. Lubarda. The onset of twinning in metals: a constitutive description. *Acta Materialia*, 49(19):4025–4039, 2001.

[66] V. V. Martynov. X-ray diffraction study of thermally and stress-induced phase transformations in single crystalline Ni-Mn-Ga alloys. *Journal de Physique IV*, 5(C8, ICOMAT, Pt.1):91–99, 1995.

[67] V. V. Kokorin, V. A. Chernenko, J. Pons, C. Segui, and E. Cesari. Acoustic phonon mode condensation in Ni_2MnGa compound. *Solid State Communications*, 101(1):7–9, 1997.

[68] N. Glavatska, V. A. L'vov, and I. Glavatskyy. Thermal phonons affecting the long-time evolution of Ni-Mn-Ga martensite under magnetic field. *Journal of Magnetism and Magnetic Materials*, 309(2):244–250, 2007.

[69] K. Ullakko, Y. Ezer, A. Sozinov, G. Kimmel, P. Yakovenko, and V. K. Lindroos. Magnetic-field-induced strains in polycrystalline Ni-Mn-Ga at room temperature. *Scripta Materialia*, 44(3):475–480, 2001.

[70] M. Chmielus, V. A. Chernenko, W. B. Knowlton, G. Kostorz, and P. Müllner. Training, constraints, and high-cycle magneto-mechanical properties of Ni-Mn-Ga magnetic shape-memory alloys. *The European Physical Journal - Special Topics*, 158(1):79–85, 2008.

[71] A. Sozinov, A. A. Likhachev, N. Lanska, O. Söderberg, K. Ullakko, and V. K. Lindroos. Stress- and magnetic-field-induced variant rearrangement in Ni-Mn-Ga single crystals with seven-layered martensitic structure. *Materials Science & Engineering, A*, A378(1-2):399–402, 2004.

[72] N. Glavatska, I. Glavatsky, Y. Ge, and V. K. Lindroos. Time-dependent dynamic response of martensite in Ni-Mn-Ga magnetic shape memory alloys to stress caused by constant magnetic field. *Journal de Physique IV: Proceedings*, 112(International Conference on Martensitic Transformations, 2002, Part 2):1009–1012, 2003. An 2003:987668; written in English.; ID: 1002.

[73] Y. Ge, H. Jiang, A. Sozinov, O. Söderberg, N. Lanska, J. Keränen, E. I. Kauppinen, V. K. Lindroos, and S. P Hannula. Crystal structure and macrotwin interface of five-layered martensite in Ni-Mn-Ga magnetic shape memory alloy. *Materials Science and Engineering: A,*, 438-440:961–964, 11/25 2006.

[74] Y. Ni and A. G. Khachaturyan. From chessboard tweed to chessboard nanowire structure during pseudospinodal decomposition. *Nature Materials*, 8:410–414, 2009.

[75] A. Böhm, S. Roth, G. Naumann, W-G. Drossel, and R. Neugebauer. Analysis of structural and functional properties of $Ni_{50}Mn_{30}Ga_{20}$ after plastic deformation. *Materials Science and Engineering: A*, 481-482:266–270, 2008.

[76] S. Besseghini, E. Villa, F. Passaretti, M. Pini, and F. Bonfanti. Plastic deformation of NiMnGa polycrystals. *Materials Science & Engineering: A*, A378(1-2):415–418, 2004.

[77] Y. Boonyongmaneerat, M. Chmielus, D. C. Dunand, and P. Müllner. Increasing magnetoplasticity in polycrystalline Ni-Mn-Ga by reducing internal constraints through porosity. *Physical Review Letters*, 99(24):247201, 2007.

[78] J. Van Humbeeck and S. Kustov. Active and passive damping of noise and vibrations through shape memory alloys: applications and mechanisms. *Smart Materials and Structures*, 14(5):S171–S185, 2005.

[79] M. A. Marioni, S. M. Allen, and R. C. O'Handley. Nonuniform twin-boundary motion in Ni-Mn-Ga single crystals. *Applied Physics Letters*, 84(20):4071–4073, 2004.

[80] K. Rolfs, A. Mecklenburg, J.-M. Guldbakke, R. C. Wimpory, A. Raatz, J. Hesselbach, and R. Schneider. Crystal quality boosts responsiveness of magnetic shape memory single crystals. *Journal of Magnetism and Magnetic Materials*, 321(8):1063–1067, 2009.

[81] A. A. Likhachev, A. Sozinov, and K. Ullakko. Modeling the strain response, magneto-mechanical cycling under the external stress, work output and energy losses in Ni-Mn-Ga. *Mechanics of Materials*, 38(5-6):551–563, 2006.

[82] R. C. O'Handley. Model for strain and magnetization in magnetic shape-memory alloys. *Journal of Applied Physics*, 83(6):3263–3270, 1998.

[83] O. Heczko, L. Straka, and S.-P. Hannula. Stress dependence of magnetic shape memory effect and its model. *Materials science and engineering A*, 438-440:1003–1006, 2006.

[84] J.-Y. Gauthier, A. Hubert, J. Abadie, N. Chaillet, and C. L'excellent. Nonlinear hamiltonian modelling of magnetic shape memory alloy based actuators. *Sensors and Actuators A: Physical*, 141(2):536–547, 2008.

[85] D. I. Paul, W. McGehee, R. C. O'Handley, and M. Richard. Ferromagnetic shape memory alloys: A theoretical approach. *Journal of Applied Physics*, 101(12):123917, 2007.

[86] V. A. L'vov, A. Kosogor, O. Söderberg, and S-P. Hannula. The symmetry-conforming theory of martensite aging. *Materials Science Forum*, 635:13–19, 2010.

[87] M. L. Richard, J. Feuchtwanger, B. Peterson, S. M. Allen, and R. C. O'Handley. Second-phase defects in Ni-Mn-Ga based ferromagnetic shape-memory alloys. *Microscopy and Microanalysis*, 12(Suppl. 2):970–971, 2006.

[88] S. Wirth, A. Leithe-Jasper, A. N. Vasil'ev, and J. M. D. Coey. Structural and magnetic properties of Ni_2MnGa. *Journal of Magnetism and Magnetic Materials*, 167(1-2):L7–L11, 1997.

[89] K. Ullakko, J. K. Huang, C. Kantner, R. C. O'Handley, and V. V. Kokorin. Large magnetic-field-induced strains in Ni_2MnGa single crystals. *Applied Physics Letters*, 69(13):1966–1968, 1996.

[90] O. Söderberg, Y. Ge, N. Glavatska, O. Heczko, K. Ullakko, and V. K. Lindroos. The behaviour of Ni-Mn-Ga martensitic alloys in magnetic field. *Journal de Physique IV: Proceedings*, 11(Pr8, Fifth European Symposium on Martensitic Transformations and Shape Memory Alloys, 2000):Pr8/287–Pr8/292, 2001.

[91] S. J. Murray, M. Marioni, S. M. Allen, R. C. O'Handley, and T. A. Lograsso. 6 % magnetic-field-induced strain by twin-boundary motion in ferromagnetic ni-mn-ga. *Applied Physics Letters*, 77(6):886–888, 2000.

[92] O. Heczko, L. Straka, and K. Ullakko. Relation between structure, magnetization process and magnetic shape memory effect of various martensites occurring in Ni-Mn-Ga alloys. *Journal de Physique IV: Proceedings*, 112(International Conference on Martensitic Transformations, 2002, Part 2):959–962, 2003.

[93] A. Sozinov, A. A. Likhachev, N. Lanska, and K. Ullakko. Giant magnetic-field-induced strain in NiMnGa seven-layered martensitic phase. *Applied Physics Letters*, 80(10):1746–1748, 2002.

[94] V. A. Chernenko, M. Chmielus, and P. Müllner. Large magnetic-field-induced strains in Ni-Mn-Ga non modulated martensite. *Applied Physics Letters*, 95(10):104103, 2009.

[95] R. C. O'Handley and S. M. Allen. *Shape memory alloys, magnetically activated ferromagnetic shape-memory materials*, pages 936–951. Encyclopedia of smart materials. J. Wiley and Sons, New York, 2002.

[96] O. Heczko and L. Straka. Temperature dependence and temperature limits of magnetic shape memory effect. *Journal of Applied Physics*, 94(11):7139–7143, 2003.

[97] C. Gomez-Polo, J. I. Perez-Landazabal, V. Recarte, V. Sanchez-Alarcos, and V. A. Chernenko. Temperature and time dependent magnetic phenomena in a nearly stoichiometric Ni_2MnGa alloy. *Journal of Physics-Condensed Matter*, 21(2):026020, 2009.

[98] L. Straka and O. Heczko. Magnetic anisotropy in Ni-Mn-Ga martensites. *Journal of Applied Physics*, 93(10, Pt. 3):8636–8638, 2003.

[99] A. A. Likhachev and K. Ullakko. The model of magnetic-field-controlled shape memory effect in NiMnGa. *Journal de Physique IV: Proceedings*, 11(Pr8, Fifth European Symposium on Martensitic Transformations and Shape Memory Alloys, 2000):Pr8/293–Pr8/298, 2001.

[100] N. Glavatska, G. Mogilniy, I. Glavatsky, S. Danilkin, D. Hohlwein, A. Beskrovnij, O. Söderberg, and V. K. Lindroos. Temperature dependence of martensite structure and its effect on magnetic-field-induced strain in Ni_2MnGa magnetic shape memory alloys. *Journal de Physique IV: Proceedings*, 112(International Conference on Martensitic Transformations, 2002, Part 2):963–967, 2003.

[101] D. A. Ruggles, E. Gans, K. P. Mohanchandra, G. P. Carman, E. Ngo, W. Nothwang, and M. W. Cole. Damping of polycrystalline Ni-Mn-Ga, bulk, pld, and sputtered thin film. *Proceedings of SPIE-The International Society for Optical Engineering*, 5387(Active Materials: Behavior and Mechanics):156–163, 2004.

[102] H. B. Xu, Y. Li, and C. B. Jiang. Ni-Mn-Ga high-temperature shape memory alloys. *Materials Science and Engineering: A*, 438-440:1065–1070, 2006.

[103] M. Wuttig, C. Craciunescu, and J. Li. Phase transformations in ferromagnetic NiMnGa shape memory films. *Materials Transactions, JIM*, 41(8):933–937, 2000.

[104] V. G. Gavriljuk, O. Söderberg, V. V. Bliznuk, N. I. Glavatska, and V. K. Lindroos. Martensitic transformations and mobility of twin boundaries in Ni_2MnGa alloys studied by using internal friction. *Scripta Materialia*, 49(8):803–809, 2003.

[105] C. Segui, E. Cesari, J. Pons, and V. Chernenko. Internal friction behavior of Ni-Mn-Ga. *Materials Science & Engineering, A*, A370(1-2):481–484, 2004.

[106] E. Gans, C. Henry, and G. P. Carman. High energy absorption in bulk ferromagnetic shape memory alloys. In D. C. Lagoudas, editor, *Smart Structures and Materials 2004, Active Materials: Behavior and mechanics*, volume 5387, pages 177–185, Bellingham, WA, USA, 2004. SPIE.

[107] M. Zeng, S. W. Or, and H. L. W. Chan. Ultrahigh anisotropic damping in ferromagnetic shape memory Ni-Mn-Ga single crystal. *Journal of Alloys and Compounds*, 493(1-2):565–568, 2010.

[108] D. C. Lagoudas, D. A. Miller, L. Rong, and P. K. Kumar. Thermomechanical fatigue of shape memory alloys. *Smart Mater. Struct.*, 18(8):085021, 2009.

[109] Feng Xiong, Yong Liu, and E. Pagounis. Thermally induced fracture of single crystal Ni-Mn-Ga ferromagnetic shape memory alloy. *Journal of Alloys and Compounds*, 415(1-2):188–192, 2006.

[110] P. Müllner, V. A. Chernenko, and G. Kostorz. A microscopic approach to the magnetic-field-induced deformation of martensite (magnetoplasticity). *Journal of Magnetism and Magnetic Materials*, 267(3):325–334, 2003.

[111] Y. Ge, O. Heczko, O. Söderberg, and S.-P. Hannula. Direct optical observation of magnetic domains in Ni-Mn-Ga martensite. *Applied Physics Letters*, 89(8):082502, 2006.

[112] S. P. Venkateswaran, N. T. Nuhfer, and M. De Graef. Anti-phase boundaries and magnetic domain structures in Ni_2MnGa-type heusler alloys. *Acta Materialia*, 55(8):2621–2636, 2007.

[113] J. Tellinen, I. Suorsa, A. Jääskeläinen, I. Aaltio, and K. Ullakko. Basic properties of magnetic shape memory actuators. In H. Borgmann, editor, *Proc. of ACTUATOR 2002*, pages 566–569, Bremen, Germany, 12. June 2002. Messe Bremen GmbH.

[114] P. Müllner, V. A. Chernenko, D. Mukherji, and G. Kostorz. Cyclic magnetic-field-induced deformation and magneto-mechanical fatigue of Ni-Mn-Ga ferromagnetic martensites. *Materials Research Society Symposium Proc.*, 785(Materials and Devices for Smart Systems):415–420, 2004.

[115] I. Aaltio and K. Ullakko. Magnetic shape memory (MSM) actuators. In H. Borgmann, editor, *Proc. ACTUATOR 2000*, pages 527–530, Bremen, Germany, 2000. Messe Bremen GmbH.

[116] I. Suorsa, J. Tellinen, E. Pagounis, I. Aaltio, and K. Ullakko. Applications of magnetic shape memory actuators. In H. Borgmann, editor, *Proc. of ACTUATOR 2002*, pages 158–161, Bremen, Germany, 12. June 2002. Messe Bremen GmbH.

[117] J. Ahola, T. Liedes, P. Kroneld, and K. Nevala. On magnetic shape memory alloy actuator characteristics. *Journal of vibroengineering*, 11(3):443–449, 2009.

[118] A. Soroka. Study of mechanical behavior evolution in 5-layered Ni-Mn-Ga magnetic shape memory single crystals during mechanical long-term cycling. Master's thesis, Aalto University, Espoo, Finland, 2010.

[119] Y. Ge, I. Aaltio, O. Söderberg, and S.-P. Hannula. X-ray diffraction reciprocal space mapping study of modulated crystal structures in 10M Ni-Mn-Ga martensitic phase. *Materials Science Forum*, 635:63–68, 2010.

[120] I. Aaltio, Y. Ge, H. Pulkkinen, A. Sjöberg, O. Söderberg, X. W. Liu, and S.-P. Hannula. Crack growth of 10M Ni-Mn-Ga material in cyclic mechanical loading. *Physics procedia*, 10:87–93, 2010.

[121] P. Molnar. *Neutron diffraction studies of martensitic transformation and deformation processes in shape memory alloys*. PhD thesis, Charles University in Prague, 2008.

[122] S. J. Murray. *Magneto-mechanical properties and applications of Ni-Mn-Ga ferromagnetic shape memory alloy*. PhD thesis, Massachusetts Institute of Technology, 2000.

[123] A. A. Likhachev, A. Sozinov, and K. Ullakko. Different modeling concepts of magnetic shape memory and their comparison with some experimental results obtained in Ni-Mn-Ga. *Materials Science & Engineering, A*, A378(1-2):513–518, 2004.

[124] A. A. Likhachev and K. Ullakko. Magnetic-field-controlled twin boundaries motion and giant magneto-mechanical effects in Ni-Mn-Ga shape memory alloy. *Physics Letters A*, 275(1,2):142–151, 2000.

[125] L. Straka and O. Heczko. Superelastic response of Ni-Mn-Ga martensite in magnetic fields and a simple model. *IEEE Transactions on Magnetics*, 39(5, Pt. 2):3402–3404, 2003.

[126] A. A. Likhachev and K. Ullakko. Magnetic-field-controlled twin boundaries motion and giant magneto-mechanical effects in Ni-Mn-Ga shape memory alloy. *Physics Letters A*, 275(1-2):142–151, 2000.

[127] S. Roth, U. Gaitzsch, M. Pötschke, and L. Schultz. Magneto-mechanical behaviour of textured polycrystals of NiMnGa ferromagnetic shape memory alloys. *Advanced materials research*, 52:29–34, 2008.

[128] P. Müllner, D. Mukherji, M. Aguirre, R. Erni, and G. Kostorz. Micromechanics of magnetic-field-induced twin-boundary motion in Ni-Mn-Ga magnetic shape-memory alloys. In J.M. Howe, D.E. Laughlin, J.K. Lee, U. Dahmen, and W.A. Soffa, editors, *Solid-to-solid phase transformations in inorganic materials*, volume 2, pages 172–185. TMS, 2005.

[129] R. W. Hertzberg. *Deformation and fracture mechanics of engineering materials*. John Wiley & Sons, Inc., New York, 3. edition, 1989.

[130] O. Heczko, K. Prokes, and S.-P. Hannula. Neutron diffraction studies of magnetic-shape memory Ni-Mn-Ga single crystal. *Journal of Magnetism and Magnetic Materials*, 316(2):386–389, 2007.

Errata

Publication VI

On page 2, on the second column rows 1 and 3 both values of T_C = 476 K should be written T_C = 376.

Ni-Mn-Ga based magnetic shape memory alloys have attracted scientific interest for more than ten years because of their exceptional properties. They can be applied e.g., for magnetic shape memory actuation and for mechanical vibration damping. The most mobile twin boundaries are found in high-quality single crystals, but their mobility often varies significantly. In the present work, twin mobility of several types of Ni-Mn-Ga single crystals is studied under shear loading as well as in monotonic uniaxial and dynamic loading at different temperatures. It is found that the stress onset for the twin boundary motion in the single martensite variant state can be more than an order of magnitude higher than in the state with existing twin boundaries between two variants. It is demonstrated that 10M Ni-Mn-Ga has potentially a long fatigue life. Factors influencing the long-term performance are proposed and discussed.

ISBN 978-952-60-4343-2 (pdf)
ISBN 978-952-60-4342-5
ISSN-L 1799-4934
ISSN 1799-4942 (pdf)
ISSN 1799-4934

Aalto University
School of Chemical Technology
Department of Materials Science and Engineering
www.aalto.fi

BUSINESS + ECONOMY

ART + DESIGN + ARCHITECTURE

SCIENCE + TECHNOLOGY

CROSSOVER

DOCTORAL DISSERTATIONS

Aalto-DD 109/2011

Ilkka Aaltio

Role of twin boundary mobility in performance of the Ni-Mn-Ga single crystals

Aalto University